Author Manuscript

Author Manuscript

Author Manuscript

Author Manuscript

HHS Public Access

Author manuscript

Cell Metab. Author manuscript; available in PMC 2023 November 01.

Published in final edited form as:

Cell Metab. 2022 November 01; 34(11): 1765–1778.e6. doi:10.1016/j.cmet.2022.09.024.

The gut peptide Reg3g links the small intestine microbiome to the regulation of energy balance, glucose levels, and gut function

Jae Hoon Shin[1], **Nadejda Bozadjieva-Kramer**[1,2], **Yikai Shao**[1,3], **Sally Lyons-Abbott**[4], **Alan C. Rupp**[5], **Darleen A. Sandoval**[1,6], **Randy J. Seeley**[1,7,*]

[1]Department of Surgery, University of Michigan, Ann Arbor, MI, USA

[2]Veterans Affairs Ann Arbor Healthcare System, Research Service, Ann Arbor, Michigan, USA

[3]Center for Obesity and Metabolic Surgery, Huashan Hospital of Fudan University, Shanghai, China

[4]Novo Nordisk Research Center Seattle, Inc., Seattle, WA, USA

[5]Department of Internal Medicine, University of Michigan, Ann Arbor, MI, USA

[6]Department of Pediatrics Section of Nutrition, University of Colorado School of Medicine, Aurora, CO, USA

[7]Lead Contact

Abstract

Changing composition of the gut microbiome is an important component of the gut adaptation to various environments, which have been implicated in various metabolic diseases including obesity and type 2 diabetes but the mechanisms by which the microbiota influence host physiology remain contentious. Here we find that both diets high in the fermentable fiber inulin and vertical sleeve gastrectomy increase intestinal expression and circulating levels of the anti-microbial peptide Reg3g. Moreover, a number of beneficial effects of these manipulations on gut function, energy balance and glucose regulation are absent in Reg3g knockout mice. Peripheral administration of various preparations of Reg3g improves glucose tolerance and this effect is dependent on the putative receptor Extl3 in the pancreas. These data suggest Reg3g acts both within the lumen and

*Correspondence: seeleyrj@med.umich.edu.

Author contributions

J.H.S. and R.J.S. conceptualized, designed, analyzed experiments and wrote the manuscript. J.H.S. and N.B.K. performed experiments. A.C.R. performed the bioinformatics analysis of the RNA-seq data. Y.S. performed the microbiota analysis. S.L. performed the expression and purification of Reg3g protein. D.A.S., and R.J.S. reviewed the manuscript. All authors read and provided feedback on manuscript and figures.

Publisher's Disclaimer: This is a PDF file of an unedited manuscript that has been accepted for publication. As a service to our customers we are providing this early version of the manuscript. The manuscript will undergo copyediting, typesetting, and review of the resulting proof before it is published in its final form. Please note that during the production process errors may be discovered which could affect the content, and all legal disclaimers that apply to the journal pertain.

Declaration of interests

R.J.S. has received research support from Novo Nordisk, Astra Zeneca, Pfizer, and Fractyl. R.J.S has served as a paid consultant and/or scientific advisory board member to Novo Nordisk, Scohia, Fractyle and ShouTi Pharma. R.J.S. has equity or option positions in Rewind and Calibrate Health. S.L. is a paid-employee of Novo Nordisk. The other authors have no financial interest to declare.

Author Manuscript Author Manuscript Author Manuscript Author Manuscript

as a gut hormone to link the intestinal microbiome to various aspects of host physiology that may be leveraged for novel treatment strategies.

Graphical Abstract

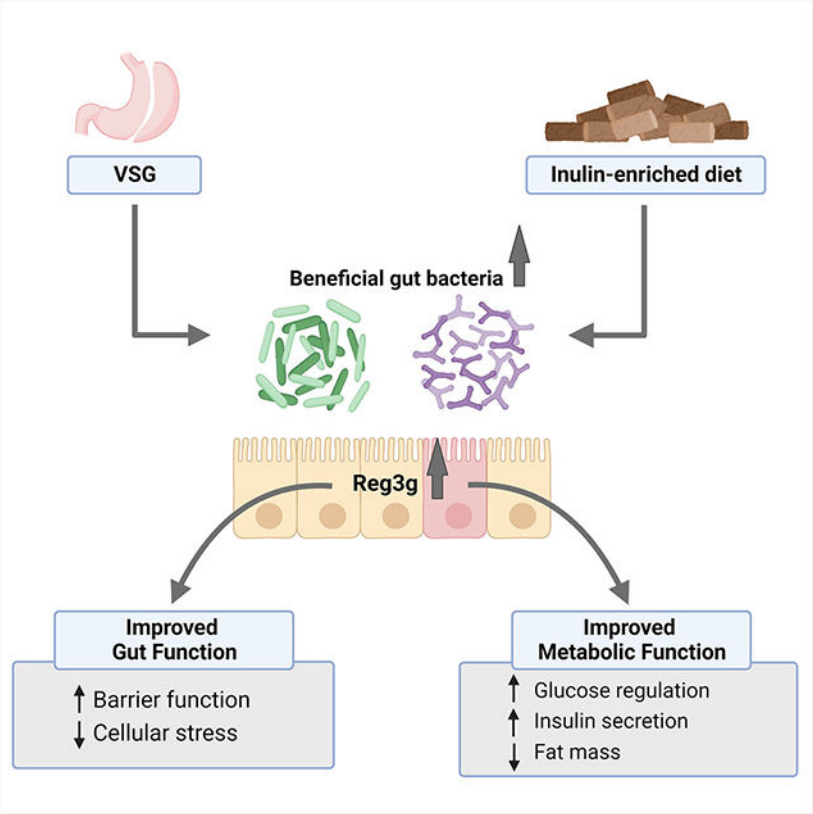

eTOC Blurb

Shin et al. find that both surgical and dietary gut manipulations increase the gut peptide Reg3g and require Reg3g for their beneficial effects on body weight, glucose levels and gut function. Reg3g may also act as a gut hormone since systemic administration improves glucose regulation via actions on the pancreas.

Introduction

Normal gut function simultaneously protects the organism from pathogens while also absorbing ingested nutrients. To achieve this balance, the gut is capable of a great deal of adaptation particularly since unlike most organs the lining of the lumen is constantly turning over. In omnivores such as humans and mice, such “enteroplasticity” is a crucial component of the gut’s ability to adapt to different diets and maintain both its barrier and absorptive functions. Of particular importance to that adaptive capability is diverse communities of microbiota that populate different segments of the GI tract. While it remains controversial, numerous studies suggest that the gut microbiota is an important component of how the gut

Author Manuscript Author Manuscript Author Manuscript Author Manuscript

impacts a number of physiological systems of the host (Altay et al., 2019; Cani et al., 2019; Rastelli et al., 2019; Sekirov et al., 2010; Turnbaugh et al., 2006).

Diets with different compositions profoundly alter gut microbiota composition (Singh et al., 2017; Zmora et al., 2019). A crucial question is whether these shifts in the bacterial populations contribute to the ability of diets to either protect from or facilitate the development of diseases such as obesity and type 2 diabetes where diet can have a profound influence (Birt et al., 2013; Lazar et al., 2019; Thingholm et al., 2019). The specific role the gut microbiome plays in obesity and type 2 diabetes has remained controversial (Rabot et al., 2010; Scheithauer et al., 2016; Scheithauer et al., 2020; Turnbaugh et al., 2006). This is at least in part because of a focus on the bacterial communities in the colon which are more easily measured in fecal samples. These communities also make up the bulk of the bacteria found in the GI tract and the focus on them would be warranted if the primary mechanism by which the bacteria impact host physiology is by the circulating levels of the various metabolites produced by these bacterial communities.

The majority of the work to absorb calories and micronutrients from ingested food, however, is done in the small intestine. Because of the need to break down and absorb different nutrients, the small intestine must be capable of more enteroplasticity compared to the large intestine. For this reason, the small intestine has received considerably more attention in understanding the role that the gut may play in the regulation of body weight and glucose levels under different circumstances. Hence, to understand the role that the microbiome plays in systemic physiology likely requires more focus on the interaction between bacteria and the systems of the small intestine. Given the smaller populations of bacteria in the small intestine, it is less likely that the primary mechanism by which the bacteria would exert effects on the host would be via changing circulating levels of bacterially-derived metabolites. Rather, it is more likely that local effects of these metabolites would impact small intestine function and signals from the gut that act on other organs to impact systemic physiology.

To this end, we took two very different interventions, one dietary and one surgical, and measured their impact on the composition of the bacterial communities in the small intestine. Both of these manipulations are associated with an increased prevalence of “healthy” bacteria. We then used probiotics to artificially boost levels of these bacteria in the small intestine. In all three experiments, there was a common effect to increase the expression and circulating levels of an anti-microbial peptide termed Reg3g (regenerating islet-derived protein 3 gamma).

As a part of the host immune system, Reg3g (the mouse homolog of human REG3A), is abundantly expressed and secreted in the small intestine where it participates in host defense via its bactericidal activity (Cash et al., 2006; Vaishnava et al., 2011). Under physiological conditions, Reg3g plays a crucial role in maintaining the host-gut microbiota segregation (Vaishnava et al., 2011). Physiologically and pharmacologically, Reg3g provides protective effects on colitis, diabetic wound healing, and alcohol-induced fatty liver disease by suppression of epithelial inflammation and bacterial colonization (Darnaud et al., 2018; Wang et al., 2016; Wu et al., 2016). This raises the possibility that Reg3g serves to connect

Author Manuscript Author Manuscript Author Manuscript Author Manuscript

changes in the small intestinal microbiome to beneficial effects on systemic physiology. Thus, we tested both the dietary and surgical interventions in Reg3g KO mice and the effect of pharmacological application of Reg3g on glucose regulation.

Results

Reg3g Is Required to Maintain Weight Loss Following VSG

Since changes in gut microbiota composition are considered a potential contributor to either metabolic perturbation or benefits, we sought to explore the role of Reg3g in various metabolic challenges. First, we found that feeding a relatively unhealthy HFD that results in weight gain and impaired glucose regulation, as well as leptin deficiency suppressed the expression of Reg3g in multiple segments of the small intestine, but Reg3g expression was unchanged in the colon (Figure S1A and S1B). As previously reported (Bluemel et al., 2018), when fed HFD to induce obesity, there were no significant differences in body weight and body composition between Reg3g KO versus WT mice (Figure S1C and S1D). Moreover, glucose tolerance with an intraperitoneal (IP) injection of dextrose showed similar glucose excursion curves between Reg3g KO and WT mice (Figure S1E).

Bariatric surgeries manipulate gut anatomy, which leads to adaptation to changes in the gut environment. Consistent with previously published RNA-seq data (Ryan et al., 2014), one of the most enriched pathways after vertical sleeve gastrectomy (VSG) in the distal small intestine were antimicrobial peptides (Figure 1A). Gene profiles belonged to the antimicrobial peptides exhibited that Reg3g is upregulated in the VSG intestine relative to Sham controls (Figure 1B). Consistent with this, both Roux-en-Y gastric bypass (RYGB) and VSG enhanced mRNA expression of Reg3g in rats and mice, respectively (Figure 1C). However, Reg3g expression after RYGB was unchanged in the duodenum, indicating that nutrient exposure is critical for increasing Reg3g expression (Figure. 1C). These findings raise the question of whether intestinal Reg3g leads to a change in circulating Reg3g levels. Although we tested multiple assays, most of them detected substantial levels in mice lacking Reg3g (Shin and Seeley, 2019). However, the Proteome Profiler Mouse Cytokines Array analysis (R&D Systems) revealed that circulating levels of Reg3g were elevated in the mice that had undergone VSG (Figure 1D and Data S1) and importantly showed no detectable circulating Reg3g in Reg3g KO mice (Data S1). To explore whether Reg3g (the mouse homolog of human REG3A) is also regulated by VSG in humans, we obtained plasma from young obese patients (14–22 years) before and at 1 and 3 months after surgery. Circulating REG3A was increased 1 and 3 months after surgery (Figure 1E). These data make a strong case that while obesity downregulates Reg3g expression, bariatric surgery is able to increase both intestinal gene expression and circulating levels of Reg3g.

To determine whether Reg3g mediates the metabolic benefits of bariatric surgery, we next performed VSG in WT and Reg3g KO mice and measured a wide range of critical endpoints. Mice were then randomly divided into 4 groups, fed 60% high-fat diet (HFD) for 8 weeks, and then underwent either VSG or sham surgery (Figure 1F). In the first 2 weeks after surgery, both WT-VSG and Reg3g KO-VSG mice lost a comparable amount of weight compared with their sham controls (Figure 1G). However, Reg3g KO-VSG mice began to gain more weight after 2 weeks and recovered body weight up to the level of

Author Manuscript Author Manuscript Author Manuscript Author Manuscript

sham-operated animals whereas WT-VSG maintained relatively lower body weight for 50 days post-surgery (Figure 1G). Body composition showed that weight change of WT-VSG after surgery was primarily due to a loss in fat mass. While WT-VSG mice had lower fat mass than Sham 8 weeks after surgery, there was no significant difference in fat mass between Reg3g KO-Sham and KO-VSG mice (Figure 1H). There was also no difference in the lean mass among the four groups both before and after surgery (Figure 1H). WT-VSG mice displayed reduced hepatic fat accumulation and triglyceride levels, but the VSG effect on hepatic fat reduction was reduced in the absence of Reg3g (Figure 1I). Furthermore, VSG significantly downregulated the expression of hepatic lipogenesis-related genes, such as SREBP1c (Srebf1), SREBP-1-regulated enzyme ACC1 (Acaca), and fatty acid translocase (CD36) but these effects of VSG were blunted in Reg3g KO mice (Figure S2).

We also examined VSG-induced changes in feeding behaviors. VSG regardless of genotype led both mice to consume less food than sham-operated mice during the recovery period up to 2 weeks after surgery, but cumulative food intake was similar over the postoperative period between WT-VSG and Reg3g KO-VSG (Figure S3A) (Frikke-Schmidt et al., 2019; Ryan et al., 2014). As time passed, cumulative food intake of all VSG mice became equivalent to Sham mice, and there was no change in the food intake among the four groups from 3-6 weeks after surgery (Figure S3A). Furthermore, when animals were given a choice between three pure macronutrient diets, both WT and Reg3g KO-VSG mice trended toward a reduced preference for fat, increased preference for carbohydrates, and no altered preference for proteins compared with sham-operated controls (Figure S3B). The deletion of Reg3g did not alter food preference not the effect of VSG to alter food preference. The gastric emptying rates determined by plasma acetaminophen levels after oral gavage, increased in both VSG groups, indicating a rapid passage of acetaminophen from the stomach into circulation compared with sham controls (Figure S3C).

Reg3g Is Required for Improvements in Glucose and Insulin Secretion Following VSG

Next, we examined whether Reg3g contributes to the improvements in glucose homeostasis that occur after VSG. VSG surgery led to a decrease in overnight-fasting blood glucose in WT mice, but this was not observed in Reg3g KO mice (Figure 2A). In response to an intraperitoneal (IP) glucose injection performed 4-weeks post-operatively, WT-VSG mice displayed a significant improvement in glucose tolerance compared to WT-Sham mice. (Figure 2B and 2C). Likewise, these effects were observed 6 weeks after surgery (Figure S4A). While an oral gavage of glucose leads to comparable levels of glucose elevation among groups (Figure 2D), WT-VSG exhibited a glucose-stimulated insulin response greater than WT-sham controls 15 min after oral gavage (Figure 2E). However, this improvement in insulin was largely absent in Reg3g KO-VSG mice (Figure 2E). In response to an oral gavage of glucose, VSG significantly increased secretion of total GLP-1 levels compared with the Sham-operated controls in both WT and Reg3g KO mice (Figure S4B). Next, we isolated islets from all groups to assess the *ex vivo* β-cell function. While islets isolated from WT-VSG mice exhibited a 2.5-fold increase in insulin secretion as compared to islets from WT-sham, glucose responsiveness in Reg3g KO-VSG islets was significantly blunted compared with their WT counterparts (Figure 2F).

Author Manuscript Author Manuscript Author Manuscript Author Manuscript

To address the direct effect of Reg3g on glucose regulation *in vivo,* HFD-fed obese mice were given an acute injection of Reg3g, followed by an intraperitoneal glucose tolerance test (IPGTT). Reg3g injection led to improved glucose tolerance compared with vehicle injection (Figure 3A). To directly test the effect of Reg3g on insulin secretion, we isolated islets from lean WT mice and measured insulin secretion. Islets treated with Reg3g displayed higher glucose-stimulated insulin secretion than those treated with vehicle (Figure 3B). This observation was further supported by repeated experiments using recombinant mouse Reg3g generated at Novo Nordisk (Figure S4C and S4D).

Does this reflect the potential for Reg3g to act as a hormone on distal organs such as the pancreas? Extl3 has been hypothesized to be a receptor for Reg3g (Wu et al., 2016). We therefore used mice in which we deleted Extl3 specifically in pancreatic β-cells expressing $Mip^{CreErt2}$ ($Extl3^{\Delta\beta\text{-cell}}$). To determine whether Extl3 is involved in Reg3g dependent glucose regulation, HFD fed male $Extl3^{\Delta\beta\text{-cell}}$ mice and their WT littermates were challenged with a single injection of Reg3g followed by an IPGTT. As expected, WT mice received Reg3g displayed better glucose tolerance as compared to PBS-treated mice (Figure 3C). Unlike WT mice, $Extl3^{\Delta\beta\text{-cell}}$ mice were insensitive to the beneficial effect of Reg3g on glucose tolerance (Figure 3D). Further analysis of the pharmacological effects of Reg3g will need to be made given that it is estimated to have a relatively short half-life. Taken together, these data highlight the necessity of Reg3g for the effects of VSG to improve glucose tolerance and glucose-stimulated insulin secretion and that at least some of these effects are mediated by hormonal rather than luminal actions of Reg3g.

Reg3g modulates microbiota composition in duodenal contents after VSG

Given the changes in gut microbiota composition as a potential contributor to the metabolic benefits of bariatric surgery (Liou et al., 2013; Sanmiguel et al., 2017), we next investigated whether Reg3g effect was associated with shifts in the microbial communities after VSG. 16S rRNA sequencing analysis of duodenal content and fecal samples was performed to determine the bacterial composition. Richness and diversity were assessed by Chao1 and Shannon index, respectively. We did not see significant differences in richness and diversity in duodenal contents. In contrast, there was a significant increase in richness and a smaller increase in feces from mice that underwent VSG compared to their respective Sham controls (Figure 4A and S5A). Principal coordinate analysis (PCoA) of UniFrac distances showed VSG had a greater effect on microbial communities in the feces compared to duodenal contents (Figure 4B and S5B). *Firmicutes* and *Bacteroidetes* were the most abundant phyla in fecal microbiota whereas they are less predominant in the duodenal contents and *Proteobacteria* and *Tenericutes* prevailed in the remainder of the duodenal microbiota (Figure 4C and S5C). Analysis of duodenal microbiota revealed the abundance of *Firmicutes* was substantially lower and the abundance of *Bacteroidetes* was higher in the duodenal content in WT-VSG mice relative to WT-Sham controls, but this was not observed in Reg3g KO-VSG mice (Figure 4C).

According to the linear discriminant analysis (LDA) effect size (LEfSe) analysis, the members of the microbial community are distinct at a different level between Sham and VSG animals (Figure 4D, 4E, S5D and S5E). To define bacteria characteristic of the

Author Manuscript Author Manuscript Author Manuscript Author Manuscript

groups, we performed a random forest analysis. The top-ranked families represented by their discriminatory importance showed that the *Lactobacillus* in Reg3g KO duodenum were the main bacteria taxon distinguishing VSG from Sham animals, but its importance was relatively mild in the WT VSG (Figure 4F). Similarly, fecal microbiotas from both groups of VSG-operated mice were enriched in *Lactobacillus* (Figure S5F). There was no genotype effect on these taxonomic changes. The relative abundance of *Lactobacillus* in duodenal contents and feces was found to be greater from VSG operated mice relative to their Sham controls (Figure 4G). Interestingly, its abundance was much higher in the duodenal microbiota from Reg3g KO-VSG mice compared with WT-VSG mice (Figure 4G).

Interaction of gut microbiota and Reg3g mediates improved gut function

Since the abundance of those bacteria relevant to producing lactate is increased after VSG, we next addressed whether VSG mediated gut microbiota alteration is associated with improvements in gut function. VSG resulted in improved gut barrier function in WT mice as reflected by a decrease in plasma FITC levels when compared with KO mice (Figure 5A). In line with this, expression levels of several cell integrity genes (i.e., ZO-1, Occludin, Cldn1) were downregulated in Reg3g KO-VSG as compared to WT counterparts (Figure 5B). Furthermore, we found that duodenal tissues from WT-VSG mice showed a trend toward higher expression of antioxidant-related genes (i.e., Sod2, Cyba, Gpx2) than those from KO-VSG mice (Figure 5C). Likewise, we also observed a trend toward a decreased levels of intestinal MDA (malondialdehyde) in obese WT mice after VSG, but VSG did not suppress MDA levels in the Reg3g KO mice (Fig. 5D). To assess the direct effect of Reg3g on cellular stress regulation in the gut, we incubated enteroids derived from Reg3g KO mice and WT littermates with the hydrogen peroxide (H_2O_2) to induce oxidative stress. Incubation of enteroids with H_2O_2 substantially increased cellular ROS production. However, ROS production was higher in enteroids lacking Reg3g compared with WT enteroids (Figure 5E). Conversely, treatment with Reg3g suppressed ROS production in both WT and Reg3g KO enteroids (Figure 5E). Together, these results suggest that VSG alters the microbiota composition including increased *Lactobacillus* which in turn, provoke the gut to make more Reg3g which leads to improvements in both gut and metabolic function.

Metabolic Effect of Dietary Inulin Supplement Is Mediated by Reg3g

Accumulating evidence suggests that dietary fiber supplements protect the host against metabolic disorders along with altering gut microbiome (Deehan et al., 2017; Makki et al., 2018). We, therefore, investigated whether Reg3g plays a role in the effect of the dietary intervention by manipulating the fiber content of HFD. Mice fed fermentable fiber enriched inulin diet which is known to enrich *Bifidobacteria* (Rossi et al., 2005; Vandeputte et al., 2017), showed increased expression of intestinal Reg3g compared to mice fed isocaloric cellulose diet (Figure 6A), implying a potential regulatory function for Reg3g in the gastrointestinal (GI) tract. To extend the role of Reg3g in metabolic homeostasis linked to fermentable fiber diet, WT and Reg3g KO mice were placed on either inulin or cellulose enriched HFD. Although mice fed inulin diet consumed less food relative to those fed cellulose diet (Figure 6B), both diets induced similar weight gain in both genotypes (Figure 6C). The inulin diet reduced body fat relative to the cellulose diet (Figure 6C). However, we observed improvements in glucose tolerance in wild-type mice fed inulin diet compared to

Author Manuscript Author Manuscript Author Manuscript Author Manuscript

that fed cellulose diet as described previously (Zou et al., 2018) whereas Reg3g KO mice were refractory to this benefit of inulin diet (Figure 6D). These results suggest that Reg3g is required for inulin diet-driven glucoregulatory improvements.

By 16S rDNA analysis in the duodenal content and fecal samples, there was no statistical difference in richness and diversity in duodenal content. However, we observed a trend toward increased richness in both VSG groups compared to their Sham controls (Figure 6E). On the other hand, the microbial richness and diversity significantly decreased in feces from inulin-fed mice compared with those in the cellulose-fed mice (Figure S6A). PCoA showed distinct separation of inulin fed mice from cellulose fed mice (Figure 6F and S6B). We further identified lower abundance of taxa belonging to *Firmicutes* and increased abundance of *Bacteroidetes, proteobacteria* and *Actinobacteria* in the duodenal content and feces of mice fed an inulin enriched diet (Figure 6G and S6C). LEfSe analysis showed more taxonomic differences in the microbiota composition of the duodenal content and fecal sample between cellulose and inulin in both WT and Reg3g KO mice (Figure 6H, 6I, S6D and S6E). Duodenal microbiota from inulin fed mice were enriched for *Bifidobacteriaceae, Bacteroidaceae* and *Sutterellaceae* at the family level (Figure 6H and 6I). Discriminatory importance scores of top-ranked genus showed that *Bifidobacterium* in duodenal contents was found significantly increased in duodenal contents from inulin-fed mice relative to cellulose fed mice in both genotypes (Figure 6J), but its importance was relatively smaller in fecal samples (Figure S6F).

Intestinal Metabolic Responses to Microbiota Are Influenced by Reg3g

As seen in VSG-mice, Inulin diet led to reduced gut permeability in WT as compared to KO mice fed inulin diet (Figure 7A). In addition, we observed that the inulin diet significantly increased expression of cell integrity (i.e., Occludin, Cldn3) and antioxidant (Sod2, Cyba, Gpx2)-associated genes in the intestine from WT mice whereas inulin effects was absent in KO mice (Figure 7B and 7C). To directly investigate whether Reg3g has an impact on the gut function of microbiota, we orally administered human-use probiotics (VSL#3) containing multiple strains of *Lactobacillus* and *Bifidobacterium* spp. to HFD-fed mice. Probiotics treatment increased both intestinal and circulating Reg3g levels (Figure 7D and 7E). Since this probiotic product contains lactic-acid-producing bacteria, we therefore examined whether lactate as a product of gut bacterial fermentation induces gut Reg3g expression. We found that lactate enhanced expression of Reg3g in intestinal enteroids and cell line in a dose dependent manner (Figure S7A and S7B). Since probiotics are used to treat a number of gut disorders and improve gut health (Pace et al., 2015; Sullivan and Nord, 2005; Wilhelm et al., 2008), we sought to determine the role of Reg3g for the protective effects of probiotics on gut barrier function. Probiotics-fed mice were given intraperitoneal (IP) injection of LPS to challenge gut permeability. Importantly, the probiotics effect on gut permeability was more pronounced in WT mice compared with mice lacking Reg3g (Figure 7E)- indicating that the microbiota-mediated gut barrier improvement at least in part depends on Reg3g. Thus, these data indicate that Reg3g is required to exert beneficial effects of direct manipulation of gut bacteria on systemic physiology.

Author Manuscript Author Manuscript Author Manuscript Author Manuscript

Discussion

A wide range of data link the status of the gut microbiome to the regulation of energy balance and glucose levels (Fujisaka et al., 2016; Gurung et al., 2020; Rosenbaum et al., 2015; Wu et al., 2017). While controversy remains, these data would indicate that a number of different manipulations of the diet and/or the gut can alter the composition of the microbiome. While most of the focus has been on changes that can be observed in fecal samples, it is clear that there are considerable changes in the microbiome of the small intestine that is likely not well represented in fecal samples (Kastl et al., 2020; Martinez-Guryn et al., 2018). Especially, the microbial community including *Lactobacillus* and *Bifidobacteria* residing in the proximal small intestine has been appreciated as metabolic regulators (Bauer et al., 2018; Donaldson et al., 2016; Shao et al., 2022). In this study, we sought to determine the links between host physiology and the gut microbiota in two highly disparate manipulations; VSG and an inulin-enriched diet that both can exert benefits on systemic metabolism and gut function.

Both a diet high in inulin and bariatric surgery have been reported to change the composition of the gut microbiome as measured in fecal or cecal samples (Kumar et al., 2016; Liou et al., 2013; Ryan et al., 2014; Vandeputte et al., 2017). Here we find that both are also associated with considerable changes in duodenal bacterial populations. Not surprisingly, there are significant differences between the two manipulations in terms of shifts in the prevalence of duodenal bacteria at the genus level. Notable in mice consuming the diet high in the soluble fiber inulin was a dramatic increase in the relative abundance of *Bifidobacteria.* In mice that receive VSG, there is a dramatic expansion of *Lactobacillus* that we have observed in multiple VSG cohorts. Both *Bifidobacteria* and *Lactobacillus* are considered “healthy” bacteria and can be found in foods and probiotics that are often used to treat various gut health issues (Linares et al., 2017; Madsen et al., 2001; Yu et al., 2015). One commonality among these “healthy” bacteria is their ability to ferment ingested carbohydrates into lactate/lactic acid (Linares et al., 2017; Masood et al., 2011). Recent studies indicate the bioactive properties of microbiota-derived lactate in stimulating Hif2a signaling, promoting stem cell proliferation and protecting from damage (Lee et al., 2018; Shao et al., 2022). Hence it is a logical hypothesis that increases in lactate connect these changes in the microbiome to the increase in expression of Reg3g. To test this hypothesis, we applied lactate to both small intestinal organoids and a transformed small intestine cell line. In both cases, application of lactate in the medium resulted in a dose-dependent increase in Reg3g expression.

Another common effect of high-fiber diets and VSG is a dramatic upregulation of Reg3g expression in the small intestine and circulation. Mice exposed to a high fat diet or leptin deficiency have reduced Reg3g expression. However, not only is expression of intestinal Reg3g increased, circulating levels are also increased after both inulin-enriched diets and VSG opening up the possibility that Reg3g may have actions both in the lumen and as a gut hormone to impact other organ systems. Reg3g is an anti-microbial peptide that plays a crucial role in maintaining the segregation of the bacterial populations in the gut from the intestinal wall and thereby contributes to the barrier function of the gut (Loonen et al., 2014; Vaishnava et al., 2011). Interestingly, the changes in the duodenum would appear to be “upstream” of the changes in the gut bacteria. First, both the ability

Author Manuscript Author Manuscript Author Manuscript Author Manuscript

of high-fiber diets to increase *Bifidobacteria* and VSG to increase *Lactobacillus* in the duodenum are not reduced in Reg3g KO mice. Hence, Reg3g is not necessary to the effect of these manipulations to increase prevalence of healthy bacteria. Second, if we provide an oral gavage of a probiotic that contains multiple strains of *Lactobacillus* the addition of *Lactobacillus* is sufficient to provoke increased expression and circulating levels of Reg3g. These *Lactobacillus*-containing probiotics have been used to treat features of leaky-gut syndrome (Ganji-Arjenaki and Rafieian-Kopaei, 2018; Le and Yang, 2018). We were able to replicate the protective effect of this probiotic against LPS-induced gut damage and this improvement was significantly reduced in Reg3g KO mice.

The implication of these results is that other manipulations that can increase Reg3g should also improve gut function in a Reg3g-dependent manner. Both inulin diets and VSG are associated with improved gut barrier function. Reg3g is necessary to these gut function changes in these effects that are absent in Reg3g KO mice. The improvement of gut-barrier function was associated with increased expression of a variety of proteins that play important roles in the tight junctions that comprise an important part of the gut barrier. These increases are also absent in Reg3g KO mice. Collectively, these results support an important role of Reg3g on gut adaptation as a result of changes in bacterial communities in the small intestine.

The next question is whether metabolic benefits of either high inulin diets or VSG require Reg3g. The degree to which bariatric surgery's ability to improve and even remit type 2 diabetes is dependent on the weight loss is still a point of considerable controversy (Chambers et al., 2011; Chondronikola et al., 2016; Courcoulas et al., 2014; Kadera et al., 2009; Yoshino et al., 2020). However, our view is that there are considerable effects of VSG that alter key aspects of glucose regulation independently of reduced body weight (Chambers et al., 2011; Douros et al., 2019). While VSG is associated with a large reduction in body weight and body fat, high-inulin diets in this paradigm produced a much smaller effect (Zou et al., 2018). Interestingly, the effect of the high-inulin diet was evident even in Reg3g KO mice while the larger effect of VSG was entirely absent in Reg3g KO mice by the time they were 8 weeks after VSG. Interestingly, both the effect of VSG and fiber diet to improve glucose tolerance were absent in Reg3g KO mice. Furthermore, post-prandial insulin secretion is tripled in VSG as compared to sham-operated mice, an effect that is observed in human as well (Bradley et al., 2014; Pok and Lee, 2014). This effect of VSG, however, was absent in Reg3g KO mice. These observations likely explain at least in part why VSG and a high inulin diet did not lead to an improvement in glucose regulation in the absence of Reg3g and point to the necessary role Reg3g plays in the effects of VSG to improve glucose regulation and increase insulin secretion.

Given that circulating levels of Reg3g are increased after these disparate manipulations, is it possible to replicate some of these effects by pharmacological application of Reg3g? Multiple preparations of Reg3g delivered acutely to DIO mice just prior to a glucose tolerance test results in a small but reliable improvement in glucose tolerance. Does this reflect the potential for Reg3g to act as a hormone on distal organs such as the pancreas? Extl3 has been hypothesized to be a receptor for Reg3g (Wu et al., 2016). Mice lacking Extl3 specifically in pancreatic islets failed to improve their glucose tolerance after acutely

Author Manuscript Author Manuscript Author Manuscript Author Manuscript

delivering Reg3g as compared to their littermate controls. Such data imply that Reg3g can have actions at sites outside the gut to have metabolically beneficial effects and provide a target receptor for these beneficial effects of Reg3g. A variety of questions remain. In particular, the nature of the intracellular signal cascade that is downstream of Extl3 and how it may interact with other known signaling systems that regulate glucose regulation downstream of GPCR's remain unknown.

In conclusion, our findings support the potential that Reg3g could be used to provide therapeutic benefit for metabolic disorders including type 2 diabetes. They also support the hypothesis that Reg3g is a mechanism by which small intestinal bacterial populations might impact host physiology. These data make clear that the ability of the gut to adapt to disparate manipulations involve changes in the gut bacteria in the small intestine that can provoke increases in Reg3g. This could influence host physiology in two ways. 1) Reg3g could be secreted as a hormone that can act directly upon other organs to alter physiology. 2) Reg3g could act within the lumen to alter gut functions such as gut barrier effectiveness that in turn impact systemic metabolism and physiology.

Limitations of Study

Our study did not include weight-matched sham-operated control to VSG mice. There is considerable controversy around the degree to which improvements in glucose regulation are secondary to weight loss but many studies point toward weight-independent effects of bariatric surgery (Abu-Gazala et al., 2018; Chambers et al., 2011; Laferrère and Pattou, 2018; Yang et al., 2022). Given that VSG failed to cause weight loss in Reg3g KO mice, it is not possible to know from the current data whether that accounts for the additional failure to improve glucose regulation and hepatic lipids. This caveat does not apply to the high fiber diets however since they produce a Reg3g-dependent effect to improve glucose that is not associated with significant weight loss. Further, acute Reg3g administration resulted in an improvement in glucose tolerance that were independent of effects on food intake and body weight. Importantly, although mice were divided into two groups by matching body weight in the experiment of acute administration, it was difficult to make the basal glucose levels equivalent between groups. Therefore, we displayed the relative glucose excursion and validated the pharmacological effect of Reg3g multiple times. Taken together, these data would support an independent role of Reg3g to regulate glucose regulation that is beyond any effects on body weight.

Another clear limitation is that it is difficult to know whether the levels of Reg3g achieved after administration of Reg3g reflect physiological levels of Reg3g. The limitations of the available assays make it impossible to measure the absolute levels of circulating Reg3g. Hence these studies provide a proof of concept that increasing levels of Reg3g can have biological effects but cannot address how regulation of Reg3g in circulation is linked to the regulation of glucose levels and insulin secretion. Assay issues also limit conclusions from our human samples before and after VSG. We cannot directly compare circulating levels of Reg3g and its human orthologue between mice and humans. There is also considerable variability in circulating levels of Reg3g between subjects. The degree this reflects alterations in Reg3g between individuals versus issues associated with the accurate

Author Manuscript Author Manuscript Author Manuscript Author Manuscript

measurement of specific Reg proteins remains to be determined. Future work will need to assess Reg3g regulation in a much broader range of patients and in a more temporally dynamic fashion.

STAR★METHODS

RESOURCE AVAILABILITY

Lead contact—Further information and requests for resources and reagents should be direct to and will be fulfilled by the Lead Contact, Randy J. Seeley (seeleyrj@med.umich.edu).

Materials availability—This study did not generate new unique reagents or materials. The analysis of the recombinant Reg3g protein used in this study have been provided in the Supplementary figures. Most mouse lines in this study are available from the Jackson Laboratory. Reg3g KO mouse and Extl3 flox/flox mouse strains are maintained at Dr. Lora V. Hooper's laboratory and Dr. Akira Sugawara respectively. They are available for transfer request with a completed Material Transfer Agreement.

EXPERIMENTAL MODEL AND SUBJECT DETAILS

Mice—Mice were single-housed under a standard 12-hour light/12-hour dark cycle with ad libitum access to water and Food (standard chow diet standard chow; Envigo Teklad or 60% HFD; Research Diet). C57BL6/J and *ob/ob* mice were purchased from the Jackson Laboratory at 6-8 weeks of age. To induce obesity, mice were fed 60% HFD for 8 weeks prior to surgery and were maintained on the same diet after surgery. Reg3g KO mice were kindly provided by Lora Hooper at the University of Texas Southwestern Medical Center (Vaishnava et al., 2011). 7-8 week-old Reg3g KO and WT male mice (all littermates) were fed 60% HFD for 8 weeks prior to surgery and returned to HFD after surgery until the end of the study. For dietary intervention, mice were fed either a high fat purified diet with 200 g cellulose or 200 g inulin per 4,057 kcals which were produced by Research Diets (New Brunswick, NJ) (Zou et al., 2018).

Human samples—Plasma of patients receiving VSG was obtained from the Pediatric Obesity Tissue Repository, Center for Bariatric Research and Innovation, at the Cincinnati Children's Hospital Medical Center. Twenty-eight obese patients with ages 14–20 were recruited. Plasma was collected before surgery and 1, and 3 months after VSG.

Study approval—All subjects recruited at Cincinnati Children's Hospital Medical Center provided written informed consent approved by the Cincinnati Children's Institutional Review Board, which reviews research in accordance with applicable federal and state regulations as well as AAHRPP accreditation standards. All animal experiments were approved by and performed according to the Institutional Animal Care and Use Committee (IACUC) of the University of Michigan in accordance with the National Institutes of Health (NIH) guidelines.

Author Manuscript Author Manuscript Author Manuscript Author Manuscript

METHOD DETAILS

Vertical sleeve gastrectomy (VSG)—HFD-fed obese mice were randomly assigned to sham and VSG groups and received surgery as previously indicated (Patel et al., 2018; Ryan et al., 2014). Briefly, all mice were exposed to the DietGel Boost (ClearH2O) before surgery. Under isoflurane anesthesia, all mice (including those receiving sham surgery) received an abdominal midline laparotomy followed by the exteriorization of the stomach. For the VSG procedure, approximately 80% of the stomach was resected along the greater curvature using an ETS35-mm staple gun (Ethicon Endo-Surgery) whereas the sham procedure involved isolating and manipulating the stomach with light pressure on the stomach using blunt forceps. Following surgery, mice were maintained on a gel diet for 4 days, solid HFD was returned on day 4. Carprofen (5mg/kg) was provided for 3 days after surgery for pain relief. The Sample size was determined based on previous studies using the VSG models (Arble et al., 2019; Ryan et al., 2014). Blood was taken from the tail vein or by cardiac puncture and collected in EDTA-coated microtubes. Among VSG operated mice, 11 out of 40 were excluded from analysis due to failure to recover from the surgery (n=1 WT, 1 KO) or from abnormal pouch formation (n= 3 WT, 9 KO). 3 out of 20 were excluded due to failure to recover from the sham surgery (n= 1 KO) or continuous weight loss (n= 2 WT). A separate Reg3g KO VSG cohort (n=4/group) fed HFD was used for the measurement of intestinal MDA and hepatic triglyceride. A cohort maintained on a chow diet was utilized for the oxidative stress study. It consists with Sham (n=7), VSG (n=6).

Glucose tolerance test—For glucose tolerance tests, mice were fasted for 5h prior to IP glucose injection (2g/kg of body weight). Blood glucose was sampled from the tip of the tail and measured at the indicated time point using a Biosen glucose and lactate analyzer (Biosen C-Line, EKF, Germany).

Macronutrient preference test—Food preference was assessed 8 weeks postoperatively in a separate cohort using a macronutrient selection paradigm (Frikke-Schmidt et al., 2019). Pure carbohydrate (Harlan Teklad; TD02521), fat (Harlan Teklad; TD02522), and protein (Harlan Teklad; TD02523) were provided in separated containers simultaneously for 7 days. Nutrition intake was monitored daily after mice were acclimatized to the containers for 3 days. Data from days 3–6 were collected, and the total caloric intake per day and the intake of each macronutrient per day were calculated and averaged over the 3 days. At the end of the study, the containers were removed, and new solid food was provided to the cages.

Intestinal permeability test—Mice were orally given with probiotics VSL#3 (2x109 CFU; Sigma-TauPharmaceuticals) daily for 2 weeks. LPS (1 mg/kg; Sigma-Aldrich) was peritoneally administered 24h before sacrifice. Intestinal permeability was assayed by oral administration of FITC-labelled dextran (10mg/100μl in PBS, Sigma-Aldrich, FD4). Mice were sacrificed 2hr after oral gavage of FITC-dextran and blood samples were collected by cardiac puncture.

Gastric emptying assessment—Six weeks after surgery, the rate of gastric emptying was assessed as previously described (Chambers et al., 2014). Briefly, after an overnight fast, 50% dextrose mixed with acetaminophen (100mg/kg, Sigma-Aldrich) was delivered

Author Manuscript Author Manuscript Author Manuscript Author Manuscript

orally. Blood was collected from the tail vein at 15 min after gavage. Plasma acetaminophen levels were measured using spectrophotometry (Sekisui Diagnostics).

Assays—Insulin levels were measured using a mouse insulin ELISA kit (Crystal Chem, 90080). GLP-1 was measured with the total GLP-1 kit (MesoScale Discovery, K150JVC-1). For GLP-1 measurement, mice from the separate cohort used for macronutrient test, were fasted for 5 hours prior to an oral administration of liquid mixed meal (200uL of Ensure Plus, Abbott Laboratories). Plasma mouse Reg3g was measured using Proteome Profiler Mouse XL Cytokine Array (R&D Systems, ARY028). Human REG3A was determined by using R-PLEX Human Reg-3-alpha Antibody Set (MesoScale Diagnostics, F21U8-3). All assays were performed according to the manufacturer's instructions. For hepatic triglyceride measurement, liver lipids were extracted with Lipid Extraction Kit (Abcam, ab211044). Triglycerides (Biovision, K622) were measured using the extracted liver lipids. Malondialdehyde (MDA) concentrations of intestines were determined using an Oxiselect TBARS assay kit (Cell Biolabs, STA-330). Cellular ROS production was determined using DCFDA/H2DCFDA assay kit (Abcam, ab113851).

RNA extraction and qRT-PCR—Total RNA was extracted using the PureLink RNA Mini Kit (Invitrogen). cDNA was synthesized by reverse transcription from mRNA using the iScript cDNA Synthesis Kit (Bio-Rad). Quantitative RT-PCR was performed with either SsoAdvanced Universal Probe Supermix (Bio-Rad) on a CFX96 Touch Real-time PCR or SYBR Green Master Mix (Applied Biosystems) on a StepONEPlus real-time PCR System (Applied Biosystems). Relative quantification of gene expression was normalized to the expression of housekeeping gene RPL32 using the $\Delta\Delta C_t$ method. Primer sequences are shown in the Table S1.

H&E staining—Tissue process for histology was performed by In Vivo Animal Core (IVAC) at the University of Michigan. Liver tissues were fixed in 4% paraformaldehyde for 24 hr. Tissues were embedded in paraffin, sliced into 4 μm sections, and stained with hematoxylin and eosin (H&E).

Islet isolation—Islets were isolated 7 weeks following surgery as described previously (Bernal-Mizrachi et al., 2010; Bernal-Mizrachi et al., 2004). Briefly, 1 mg/mL of collagenase (Roche) was dissolved in Hank's Buffer. The junction of the common bile duct to the duodenum was closed using a clamp. Approximately 5 mL of collagenase solution was injected slowly into the common bile duct of each mouse. After injecting the collagenase solution, the pancreas was dissected and placed in a tube and incubated in water bath at 37°C for 12-16 minutes for further digestion. The digested pancreas was washed multiple times with Hanks's Buffer supplemented with 10% FBS and passed through a strainer to eliminate undigested parts. Finally, the digested pancreas was passed through 70μm filter (Thermo Fisher Scientific) to collect islets. The islets were handpicked into RPMI media containing 5mM glucose and incubated overnight in a cell culture incubator (37°C, 5% CO_2).

***Ex vivo* glucose-stimulated insulin secretion:** After overnight incubation, islets were pre-cultured in Krebs-Ringer (KRBB) medium containing 6 mM glucose and 0.2% BSA for

Author Manuscript Author Manuscript Author Manuscript Author Manuscript

1 hour. Groups of 10 islets/mouse were placed in 8 μm cell culture inserts (Milli cell, Millipore), pre-incubated in HG KRBB (6 mM glucose) for 1-2 hours. Glucose-stimulated insulin secretion was conducted by treating islets consecutively with 2mM glucose and 12mM glucose for 30 min per condition. Assessment of insulin content of the islets was performed by extraction in 20 μ protein lysis buffer (Sigma-Aldrich) per 10 islets/insert after each assay. All assays represent results from 2 independent experiments. Secreted insulin levels and islet insulin content were measured with a mouse Insulin ELISA kit (Crystal Chem). All data is represented as secreted insulin in the culture medium normalized to islet insulin content for each insert of islets and presented as fold change compared to control.

***In vivo* and *ex vivo* treatment:** Recombinant mouse Reg3g (R&D) was administered intraperitoneally 20 min prior to glucose bolus with the dose indicated in the figure legends. Enteroids and islets were treated with Reg3g (50 or 100 ng/ml).

RNA sequencing analysis—FASTQ files associated with GEO accession number GSE53782 were downloaded from the SRA using fastq-dump (runs: SRR1068180, SRR1068181, SRR1068182, SRR1068183, SRR1068184, SRR1068185, SRR1068186, SRR1068187, SRR1068188, SRR1068189). Metadata was accessed from SRA Run Selector for BioProject PRJNA232938 (SraRunTable.txt).

A mouse genome index was generated using STAR 2.7.3a with default parameters from the Ensembl v99 genome FASTA file (Mus_musculus.GRCm38.dna.primary assembly.fa) and GTF file (Mus_musculus.GRCm38.99.gtf). FASTQ files were then mapped to the genome using STAR 2.7.3a with default parameters and a count matrix was generated with the quantMode GeneCounts flag. Count matrix files were analyzed in R 3.6.3. Estimated fold-change and associated P values were calculated using DESeq2 1.26.0 (and corroborated using edgeR 3.28.1). Heatmaps were generated for genes of interest by generating sample z-scores of the log2(CPM+1) expression levels for each gene. For pathway analysis, differentially expressed genes were divided into 3 categories: (1) genes with FDR < 0.05 in both DESeq2 & edgeR (3 genes), (2) genes with P (uncorrected) < 0.05 in both DESeq2 & edgeR (629 genes), (3) genes with a > 1.5 fold-change by both DESeq2 & edgeR and whose expression > 1 counts per million in the median sample (835 genes). These gene lists were converted to Entrez ID using AnnotationDbi 1.48.0 and org.Mm.eg.db 3.10.0 and then fed into pathway enrichment analysis (ReactomePA 1.30.0 function enrichPathway).

DNA extraction and 16S rRNA sequencing—Duodenal contents and fecal pellets were added to each well of the Bead plate and the microbiota community analysis was conducted through 16S rRNA gene sequencing by the Microbiome Core in the Microbial Systems Molecular Biology Laboratories at the University of Michigan. DNA was isolated using MagAttract PowerMicrobiome kit DNA/RNA kit (Qiagen) on the EpMotion 5075 (Eppendorf) liquid handler. Extracted DNA is then used to generate 16S rRNA libraries for community analysis. The DNA libraries were prepared by the Microbiome Core as described previously (Seekatz et al., 2015). Briefly, DNA was PCR amplified using a set of barcoded dual-index primers specific to the V4 region of the 16S rRNA gene (Kozich et al., 2013). The Agilent Bioanalyzer is used to confirm the size of the amplicon library (~399 bp) using a high-sensitive DNA analysis kit (Agilent). Pooled amplicon library is

Author Manuscript Author Manuscript Author Manuscript Author Manuscript

then sequenced on the Illumina MiSeq platform using the 500 cycle MiSeq V2 Reagent kit (Illumina) according to the manufacturer's instructions with modifications of the primer set with custom read 1/read 2 and index primers added to the reagent cartridge. The “Preparing Libraries for Sequencing on the MiSeq” (part 15039740, Rev. D) protocol was used to prepare libraries with a final load concentration of 5.5 pM, spiked with 15% PhiX to create diversity within the run. FASTQ files are generated when the 2 x 250 bp sequencing completes.

Following sequencing, microbiome bioinformatics were run using QIIME 2 2020.2 (Bolyen et al., 2019) according to the online tutorials (https://docs.qiime2.org/2020.2/tutorials/). Briefly, non-singleton amplicon sequence variants (ASVs, 100% operational taxonomic units (OTUs)) were generated from raw sequences after trimming with the cutadapt plugin (Martin, 2011) and denoising with the dada2 plugin (Callahan et al., 2016). Taxonomy was then assigned to ASVs using the classify-sklearn alignment algorithm (Bokulich et al., 2018) against the Greengenes database (Release 13.8) of 99% OTUs reference sequences (McDonald et al., 2012). Alpha diversity metrics including Chao1 (Chao, 1984) and Shannon (Shannon, 1948), which estimate with-in sample richness and diversity respectively, were calculated using the diversity plugin. Linear discriminant analysis (LDA) effect size (LEfSe) with default parameters (Segata et al., 2011) and Random Forest Classifier with 10-fold cross-validations (Breiman, 2001) were computed to identify significantly different microbes in abundance between groups at different taxonomic levels.

Recombinant Reg3g—Lyophilized recombinant mouse Reg3g protein was purchased from R&D Systems (8189-RG) and resuspended in PBS (1 mM KH2PO4, 3 mM Na2HPO4, 155 mM NaCl pH 7.2) at a concentration of 0.48 mg/mL and 20ug/mL. After filtration through a 0.2uM filter analysis with SDS-PAGE, endotoxin, analytical size exclusion and LC-MS was performed (Data S2).

Expression and purification of recombinant Reg3g—For recombinant expression, synthetic sequences encoding mouse Reg3g (Uniprot O09049 E27-A174) was cloned into an E. coli expression vector encoding a N-terminal HQ6 fusion tags and an HRV protease site with expression under the control of the T7 promoter. The native signal peptide as predicted by SignalP was not included, yielding a final sequence of E27-A174. GenElute Endofree maxi prep kits (Sigma NA0410-1KT) were used to generate higher amounts of plasmid DNA for scale up production efforts. The E. coli host codon optimized plasmid was transformed into BL21-CodonPlus (DE3)-RIPL cells for expression. One mL overnight culture was innoculated into 10ml of LB media + 1%glucose + carb (Teknova) and incubated 6 hours at 37°C. After the 6-hour incubation the 10ml culture was used to innoculate 1L of superbroth+carb + autoinduction supplement (Teknova), grown at 37oC with shaking at 250rpm for 16 hours. Inclusion bodies (12g) were resuspended in 10X (120mL) 20mM Tris pH7.5, 10mM EDTA pH8 + 120ul (~1/1000x) lysonase. The resuspension mixture was solubilized further by homogenizer and incubated on ice for 30min. A final lysis was performed by one pass through a cell disruptor at 30psi, followed by centrifugation at 10,000g for 30min for clarification. The inclusion body pellet was resuspended in 50ml of 20mM Tris pH7.5, 10mM EDTA pH8, 1% TX-100, mixed by

Author Manuscript Author Manuscript Author Manuscript Author Manuscript

homogenizer, then followed by a centrifugation at 10,000g for 10 min. This wash was repeated once, followed by a wash by resuspension in 50ml of H2O, mixed by homogenizer, followed by centrifugation at 10,000g for 10min. The washed pellet was resuspended in 10ml of 7M Gu-HCl, 5mM DTT, 100mM Tris, pH8. The resuspended pellet was mixed by homogenizer, followed by rotating at room temperature for 2 hours to further dissolve the pellet, with a final yield of 35 mg/ml.

To refold Reg3g 5mL of the solubilized inclusion bodies was added dropwise while stirring to 500ml of refold solution (50mM Tris, 2mM Ca++, 2M Urea, 3mM Red Glu: 0.6mM Ox Glu, pH 9). The mixture was stirred overnight at room temperature and then filtered through a 0.2uM filter. The refold mixture was diluted 1:1 with H20 and then loaded onto 2x5ml Ni excel columns (GE) in 25mM Tris, 25mM NaCl, 2mM Ca, pH7.5., at a rate of 5ml/min. The columns were washed with 20mL of 50mM Tris, 2mM Ca++, 2M Urea, 3mM Red Glu: 0.6mM Ox Glu, final pH 9 (2CV) followed by a TX wash of 200mL PBS, 0.05% TX100, 0.05% TX114 (20CV). This was followed by a 200mL PBS wash (pH 7.2) (20CV), followed by an elution in 25mL of PBS, 300mM Imidazole, 300mM L-Arg, pH 7.5 (2.5CV).

Selected fractions were pooled from the eluent and quantitated by nanodrop as a concentration of 4.5mg/ml with a final amount of 90mg in 20ml_. The HQ6 tag was removed by HRV protease digestion with the addition of 0.9mg HRV to the pooled fractions, followed by an overnight incubation at 4°C (1:10 dilution). After digestion the mixture was loaded on a 320mL S75 column (GE) in PBS pH 7.2. Selected S75 fractions were pooled for subtractive IMAC to remove both the HRV and the HQ tag from the Reg3g protein. Fractions were applied to 2 5mL Ni excel columns (GE) in PBS pH 7.2. The flow through containing the Reg3g was collected, followed by an elution of the HQ tag and HRV elution with 300mM Imidazole, 300mM L-Arg, pH 7.5. The Reg3g protein was 0.2uM filtered with a final concentration of 2.04mg/mL, followed by analysis with SDS-PAGE, endotoxin, analytical size exclusion and LC-MS (Data S2).

Recombinant protein analysis—LC/MS analysis was performed using an Agilent 1290 Infinity II UHPLC system coupled to an Agilent 6545 Q-TOF. LC separations were performed on a Zorbax 300-Diphenyl column (Agilent, 1.8 μm, 300 Å) with a flow rate of 0.4 ml/min used with a solvent gradient of 30% to *70%* B in 6 minutes. Solvent A was 0.1% (v/v) formic acid in water and the composition of solvent B was 0.1% (v/v) formic acid in 100% acetonitrile. The mass spectrometer was operated in positive ion mode with a full-scan MS spectra from 400 to 3,200 m/z. Analytical size exclusion was performed using an Agilent UPLC HP1290 system using gel filtration standards (BioRad 1511901). Separations were performed on a Waters BEH column, 1.7 μm, 200 Å, 4.6 mm ID x 150 mm L with a flow rate of 0.35 ml/minute in 10 minutes. The mobile phase was 20 mM Phosphate, 150 mM NaCl, 2% Isopropanol, pH 7. Endotoxin testing was performed as per the manufacturer's instructions (Charles River PTS Endosafe Assay). Protein stability was tested by three freeze thaws at −80C and overnight incubation at 37°C, with those samples compared to an untreated sample. Calculated main peak on analytical size exclusion was selected as the indicator of protein stability (Data S3). According to the bioanalysis, the mouse Reg3g proteins will have a half-life of <2 min and there is a DPP4 substrate site on the N' terminus of the protein.

Author Manuscript Author Manuscript Author Manuscript Author Manuscript

QUANTIFICATION AND STATISTICAL ANALYSIS

Statistical analysis was performed using GraphPad Prism (GraphPad Software). Data are presented as mean ± standard error of mean (SEM). Statistical significance was determined by the methods specified in each individual figure legend. Two group comparisons were analyzed using two-tailed Student's t tests. Multiple comparisons were assessed by one-way or two-way analyses of variance (ANOVA) followed by post hoc test. Significance was defined as *P < 0.05, **P < 0.01, and ***P < 0.001.

Data and code availability

- RNA-seq data have been deposited in the NCBI Gene Expression Omnibus under accession number GEO: GSE53782. This paper does not report original code.
- The raw data and original blot image supporting the conclusions of this manuscript can be found in Data S1 - Source Data. The analysis of recombinant protein used in this manuscript can be found in Data S2 - Recombinant Reg3g.
- Any additional information required to reanalyze the data reported in this work paper is available from the lead contact upon request

Supplementary Material

Refer to Web version on PubMed Central for supplementary material.

Acknowledgments

The authors thank Alfor Lewis, Andriy Myronovych, Mouhamadoul Toure for technical assistance in performing the vertical sleeve gastrectomy, Kelli Rule for assistance in mouse breeding, Ayesha Misquith for technical assistance in optimizing the expression and purification of the protein, and Dr. Allison Kowalsky for critical review of the manuscript. Reg3g knockout mice and Extl3 flox/flox mice were kindly provided by Dr. Lora V Hooper (University of Texas Southwestern Medical Center, Dallas, TX, USA) and Dr. Akira Sugawara (Tohoku University School of Medicine) respectively. We also would like to acknowledge the Pediatric Obesity Tissue Repository (POTR) co-investigators Thomas Inge, MD, PhD, Todd Jenkins PhD and Stavra Xanthakos MD and the coordinators who helped with this human biospecimen banking including Lindsey Shaw, Rosemary Miller, and Jennifer Black. This study was supported in part by NIH grants R01DK107652, R01DK133140 and P01DK117821 (to R.J.S.), R01DK107282 and R01DK121995 (to D.A.S.), UL1TR002240, 5T32DK108740, and 5P30DK034933 (to N.B.K.) and Department of Veterans Affairs IK2BX005715 (to N.B.K.), funded by the China government (China Scholarship Council grant; CSC#201606100218 and National Natural Science Foundation; NNSF#82100584 to Y.S.) and by Basic Science Research Program through the National Research Foundation of Korea (Ministry of Education; 2018R1A6A3A03011269; J.H.S.). This work is also supported in part by NIH-funded Michigan Nutrition and Obesity Research Center (MNORC) P30DK089503, Michigan Mouse Metabolic Phenotyping Center (MMPC) 5U2CDK110768, the American Diabetes Association; 1-19-IBS-252 (to D.A.S.), and by NIDDK Information Network's (dkNET) New Investigator Pilot Program in Bioinformatics U24DK097771 (to A.C.R.)

References

Abu-Gazala S, Horwitz E, Ben-Haroush Schyr R, Bardugo A, Israeli H, Hija A, Schug J, Shin S, Dor Y, Kaestner KH, et al. (2018). Sleeve Gastrectomy Improves Glycemia Independent of Weight Loss by Restoring Hepatic Insulin Sensitivity. Diabetes 67, 1079–1085 [PubMed: 29475831]

Altay O, Nielsen J, Uhlen M, Boren J, and Mardinoglu A (2019). Systems biology perspective for studying the gut microbiota in human physiology and liver diseases. EBioMedicine 49, 364–373. [PubMed: 31636011]

Arble DM, Evers SS, Bozadjieva N, Frikke-Schmidt H, Myronovych A, Lewis A, Toure MH, and Seeley RJ (2018). Metabolic comparison of one-anastomosis gastric bypass, single-anastomosis

Author Manuscript Author Manuscript Author Manuscript Author Manuscript

duodenal-switch, Roux-en-Y gastric bypass, and vertical sleeve gastrectomy in rat. Surg Obes Relat Dis 14, 1857–1867. [PubMed: 30292648]

Birt DF, Boylston T, Hendrich S, Jane JL, Hollis J, Li L, McClelland J, Moore S, Phillips GJ, Rowling M, et al. (2013). Resistant starch: promise for improving human health. Adv Nutr 4, 587–601. [PubMed: 24228189]

Bluemel S, Wang L, Martino C, Lee S, Wang Y, Williams B, Horvath A, Stadlbauer V, Zengler K, and Schnabl B (2018). The Role of Intestinal C-type Regenerating Islet Derived-3 Lectins for Nonalcoholic Steatohepatitis. Hepatol Commun 2, 393–406. [PubMed: 29619418]

Bradley D, Magkos F, Eagon JC, Varela JE, Gastaldelli A, Okunade AL, Patterson BW, and Klein S (2014). Matched weight loss induced by sleeve gastrectomy or gastric bypass similarly improves metabolic function in obese subjects. Obesity (Silver Spring) 22, 2026–2031. [PubMed: 24891156]

Cani PD, Van Hul M, Lefort C, Depommier C, Rastelli M, and Everard A (2019). Microbial regulation of organismal energy homeostasis. Nat Metab 1, 34–46. [PubMed: 32694818]

Cash HL, Whitham CV, Behrendt CL, and Hooper LV (2006). Symbiotic bacteria direct expression of an intestinal bactericidal lectin. Science (New York, N.Y.) 313, 1126–1130.

Chambers AP, Jessen L, Ryan KK, Sisley S, Wilson-Perez HE, Stefater MA, Gaitonde SG, Sorrell JE, Toure M, Berger J, et al. (2011). Weight-independent changes in blood glucose homeostasis after gastric bypass or vertical sleeve gastrectomy in rats. Gastroenterology 141, 950–958. [PubMed: 21699789]

Chondronikola M, Harris LL, and Klein S (2016). Bariatric surgery and type 2 diabetes: are there weight loss-independent therapeutic effects of upper gastrointestinal bypass? J Intern Med 280, 476–486. [PubMed: 27739136]

Courcoulas AP, Goodpaster BH, Eagleton JK, Belle SH, Kalarchian MA, Lang W, Toledo FG, and Jakicic JM (2014). Surgical vs medical treatments for type 2 diabetes mellitus: a randomized clinical trial. JAMA Surg 149, 707–715. [PubMed: 24899268]

Darnaud M, Dos Santos A, Gonzalez P, Augui S, Lacoste C, Desterke C, De Hertogh G, Valentino E, Braun E, Zheng J, et al. (2018). Enteric Delivery of Regenerating Family Member 3 alpha Alters the Intestinal Microbiota and Controls Inflammation in Mice With Colitis. Gastroenterology 154, 1009–1023. [PubMed: 29133078]

Deehan EC, Duar RM, Armet AM, Perez-Muñoz ME, Jin M, and Walter J (2017). Modulation of the Gastrointestinal Microbiome with Nondigestible Fermentable Carbohydrates To Improve Human Health. Microbiol Spectr 5.

Donaldson GP, Lee SM, and Mazmanian SK (2016). Gut biogeography of the bacterial microbiota. Nat Rev Microbiol. 14, 20–32. [PubMed: 26499895]

Douros JD, Niu J, Sdao S, Gregg T, Fisher-Wellman K, Bharadwaj M, Molina A, Arumugam R, Martin M, Petretto E, et al. (2019). Sleeve gastrectomy rapidly enhances islet function independently of body weight. JCI Insight 4.

Frikke-Schmidt H, Hultman K, Galaske JW, Jørgensen SB, Myers MG Jr., and Seeley RJ (2019). GDF15 acts synergistically with liraglutide but is not necessary for the weight loss induced by bariatric surgery in mice. Mol Metab 21, 13–21. [PubMed: 30685336]

Fujisaka S, Ussar S, Clish C, Devkota S, Dreyfuss JM, Sakaguchi M, Soto M, Konishi M, Softic S, Altindis E, et al. (2016). Antibiotic effects on gut microbiota and metabolism are host dependent. J Clin Invest 126, 4430–4443. [PubMed: 27775551]

Ganji-Arjenaki M, and Rafieian-Kopaei M (2018). Probiotics are a good choice in remission of inflammatory bowel diseases: A meta analysis and systematic review. J Cell Physiol 233, 2091–2103. [PubMed: 28294322]

Gurung M, Li Z, You H, Rodrigues R, Jump DB, Morgun A, and Shulzhenko N (2020). Role of gut microbiota in type 2 diabetes pathophysiology. EBioMedicine 51, 102590. [PubMed: 31901868]

Kadera BE, Lum K, Grant J, Pryor AD, Portenier DD, and DeMaria EJ (2009). Remission of type 2 diabetes after Roux-en-Y gastric bypass is associated with greater weight loss. Surg Obes Relat Dis 5, 305–309. [PubMed: 19460674]

Kastl AJ Jr., Terry NA, Wu GD, and Albenberg LG (2020). The Structure and Function of the Human Small Intestinal Microbiota: Current Understanding and Future Directions. Cell Mol Gastroenterol Hepatol 9, 33–45. [PubMed: 31344510]

Author Manuscript Author Manuscript Author Manuscript Author Manuscript

Kumar SA, Ward LC, and Brown L (2016). Inulin oligofructose attenuates metabolic syndrome in high-carbohydrate, high-fat diet-fed rats. Br J Nutr 116, 1502–1511. [PubMed: 27805541]

Laferrère B, and Pattou F (2018). Weight-Independent Mechanisms of Glucose Control After Roux-en-Y Gastric Bypass. Front Endocrinol (Lausanne). 9, 530. [PubMed: 30250454]

Lazar V, Ditu LM, Pircalabioru GG, Picu A, Petcu L, Cucu N, and Chifiriuc MC (2019). Gut Microbiota, Host Organism, and Diet Trialogue in Diabetes and Obesity. Front Nutr 6, 21. [PubMed: 30931309]

Le B, and Yang SH (2018). Efficacy of Lactobacillus plantarum in prevention of inflammatory bowel disease. Toxicology reports 5, 314–317. [PubMed: 29854599]

Lee YS, Kim TY, Kim Y, Lee SH, Kim S, Kang SW, Yang JY, Baek IJ, Sung YH, Park YY, et al. (2018). Microbiota-Derived Lactate Accelerates Intestinal Stem-Cell-Mediated Epithelial Development. Cell Host Microbe 24, 833–846.e836. [PubMed: 30543778]

Linares DM, Gómez C, Renes E, Fresno JM, Tornadijo ME, Ross RP, and Stanton C (2017). Lactic Acid Bacteria and Bifidobacteria with Potential to Design Natural Biofunctional Health-Promoting Dairy Foods. Front Microbiol 8, 846. [PubMed: 28572792]

Liou AP, Paziuk M, Luevano J-M Jr., Machineni S, Turnbaugh PJ, and Kaplan LM (2013). Conserved shifts in the gut microbiota due to gastric bypass reduce host weight and adiposity. Science translational medicine 5, 178ra141–178ra141.

Loonen LMP, Stolte EH, Jaklofsky MTJ, Meijerink M, Dekker J, van Baarlen P, and Wells JM (2014). REG3γ-deficient mice have altered mucus distribution and increased mucosal inflammatory responses to the microbiota and enteric pathogens in the ileum. Mucosal immunology 7, 939–947. [PubMed: 24345802]

Madsen K, Cornish A, Soper P, McKaigney C, Jijon H, Yachimec C, Doyle J, Jewell L, and De Simone C (2001). Probiotic bacteria enhance murine and human intestinal epithelial barrier function. Gastroenterology 121, 580–591. [PubMed: 11522742]

Makki K, Deehan EC, Walter J, and Bäckhed F (2018). The Impact of Dietary Fiber on Gut Microbiota in Host Health and Disease. Cell host & microbe 23, 705–715. [PubMed: 29902436]

Martinez-Guryn K, Hubert N, Frazier K, Urlass S, Musch MW, Ojeda P, Pierre JF, Miyoshi J, Sontag TJ, Cham CM, et al. (2018). Small Intestine Microbiota Regulate Host Digestive and Absorptive Adaptive Responses to Dietary Lipids. Cell Host Microbe 23, 458–469.e455. [PubMed: 29649441]

Masood MI, Qadir MI, Shirazi JH, and Khan IU (2011). Beneficial effects of lactic acid bacteria on human beings. Crit Rev Microbiol 37, 91–98. [PubMed: 21162695]

Pace F, Pace M, and Quartarone G (2015). Probiotics in digestive diseases: focus on Lactobacillus GG. Minerva Gastroenterol Dietol 61, 273–292. [PubMed: 26657927]

Pok EH, and Lee WJ (2014). Gastrointestinal metabolic surgery for the treatment of type 2 diabetes mellitus. World J Gastroenterol 20, 14315–14328. [PubMed: 25339819]

Rabot S, Membrez M, Bruneau A, Gérard P, Harach T, Moser M, Raymond F, Mansourian R, and Chou CJ (2010). Germ-free C57BL/6J mice are resistant to high-fat-diet-induced insulin resistance and have altered cholesterol metabolism. Faseb j 24, 4948–4959. [PubMed: 20724524]

Rastelli M, Cani PD, and Knauf C (2019). The Gut Microbiome Influences Host Endocrine Functions. Endocr Rev 40, 1271–1284. [PubMed: 31081896]

Rosenbaum M, Knight R, and Leibel RL (2015). The gut microbiota in human energy homeostasis and obesity. Trends Endocrinol Metab 26, 493–501. [PubMed: 26257300]

Rossi M, Corradini C, Amaretti A, Nicolini M, Pompei A, Zanoni S, and Matteuzzi D (2005). Fermentation of fructooligosaccharides and inulin by bifidobacteria: a comparative study of pure and fecal cultures. Appl Environ Microbiol 71, 6150–6158. [PubMed: 16204533]

Ryan KK, Tremaroli V, Clemmensen C, Kovatcheva-Datchary P, Myronovych A, Karns R, Wilson-Pérez HE, Sandoval DA, Kohli R, Bäckhed F, et al. (2014). FXR is a molecular target for the effects of vertical sleeve gastrectomy. Nature 509, 183–188. [PubMed: 24670636]

Sanmiguel CP, Jacobs J, Gupta A, Ju T, Stains J, Coveleskie K, Lagishetty V, Balioukova A, Chen Y, Dutson E, et al. (2017). Surgically Induced Changes in Gut Microbiome and Hedonic Eating as Related to Weight Loss: Preliminary Findings in Obese Women Undergoing Bariatric Surgery. Psychosom Med 79, 880–887. [PubMed: 28570438]

Author Manuscript Author Manuscript Author Manuscript Author Manuscript

Scheithauer TP, Dallinga-Thie GM, de Vos WM, Nieuwdorp M, and van Raalte DH (2016). Causality of small and large intestinal microbiota in weight regulation and insulin resistance. Mol Metab 5, 759–770. [PubMed: 27617199]

Scheithauer TPM, Rampanelli E, Nieuwdorp M, Vallance BA, Verchere CB, van Raalte DH, and Herrema H (2020). Gut Microbiota as a Trigger for Metabolic Inflammation in Obesity and Type 2 Diabetes. Front Immunol 11, 571731. [PubMed: 33178196]

Sekirov I, Russell SL, Antunes LC, and Finlay BB (2010). Gut microbiota in health and disease. Physiol Rev 90, 859–904. [PubMed: 20664075]

Shao Y, Evers SS, Shin JH, Ramakrishnan SK, Bozadjieva-Kramer N, Yao Q, Shah YM, Sandoval DA, and Seeley RJ (2022). Vertical sleeve gastrectomy increases duodenal Lactobacillus spp. richness associated with the activation of intestinal HIF2α signaling and metabolic benefits. Mol Metab 57, 101432. [PubMed: 34998940]

Shin JH, and Seeley RJ (2019). Reg3 Proteins as Gut Hormones? Endocrinology 160, 1506–1514. [PubMed: 31070724]

Singh RK, Chang HW, Yan D, Lee KM, Ucmak D, Wong K, Abrouk M, Farahnik B, Nakamura M, Zhu TH, et al. (2017). Influence of diet on the gut microbiome and implications for human health. J Transl Med 15, 73. [PubMed: 28388917]

Sullivan A, and Nord CE (2005). Probiotics and gastrointestinal diseases. J Intern Med 257, 78–92. [PubMed: 15606379]

Thingholm LB, Rühlemann MC, Koch M, Fuqua B, Laucke G, Boehm R, Bang C, Franzosa EA, Hübenthal M, Rahnavard A, et al. (2019). Obese Individuals with and without Type 2 Diabetes Show Different Gut Microbial Functional Capacity and Composition. Cell Host Microbe 26, 252–264.e210. [PubMed: 31399369]

Turnbaugh PJ, Ley RE, Mahowald MA, Magrini V, Mardis ER, and Gordon JI (2006). An obesity-associated gut microbiome with increased capacity for energy harvest. Nature 444, 1027–1031. [PubMed: 17183312]

Vaishnava S, Yamamoto M, Severson KM, Ruhn KA, Yu X, Koren O, Ley R, Wakeland EK, and Hooper LV (2011). The antibacterial lectin RegIIIgamma promotes the spatial segregation of microbiota and host in the intestine. Science 334, 255–258. [PubMed: 21998396]

Vandeputte D, Falony G, Vieira-Silva S, Wang J, Sailer M, Theis S, Verbeke K, and Raes J (2017). Prebiotic inulin-type fructans induce specific changes in the human gut microbiota. Gut 66, 1968–1974. [PubMed: 28213610]

Wang L, Fouts DE, Starkel P, Hartmann P, Chen P, Llorente C, DePew J, Moncera K, Ho SB, Brenner DA, et al. (2016). Intestinal REG3 Lectins Protect against Alcoholic Steatohepatitis by Reducing Mucosa-Associated Microbiota and Preventing Bacterial Translocation. Cell host & microbe 19, 227–239. [PubMed: 26867181]

Wilhelm SM, Brubaker CM, Varcak EA, and Kale-Pradhan PB (2008). Effectiveness of probiotics in the treatment of irritable bowel syndrome. Pharmacotherapy 28, 496–505. [PubMed: 18363533]

Wu H, Esteve E, Tremaroli V, Khan MT, Caesar R, Mannerås-Holm L, Ståhlman M, Olsson LM, Serino M, Planas-Fèlix M, et al. (2017). Metformin alters the gut microbiome of individuals with treatment-naive type 2 diabetes, contributing to the therapeutic effects of the drug. Nat Med 23, 850–858. [PubMed: 28530702]

Wu Y, Quan Y, Liu Y, Liu K, Li H, Jiang Z, Zhang T, Lei H, Radek KA, Li D, et al. (2016). Hyperglycaemia inhibits REG3A expression to exacerbate TLR3-mediated skin inflammation in diabetes. Nat Commun 7, 13393–13393. [PubMed: 27830702]

Yang P, Bonham AJ, Ghaferi AA, and Varhan OA (2022). Comparing Diabetes Outcomes: Weight-independent effects of sleeve gastrectomy versus matched patients with similar weight loss. Ann Surg. 275, 924–927. [PubMed: 33201112]

Yoshino M, Kayser BD, Yoshino J, Stein RI, Reeds D, Eagon JC, Eckhouse SR, Watrous JD, Jain M, Knight R, et al. (2020). Effects of Diet versus Gastric Bypass on Metabolic Function in Diabetes. N Engl J Med 383, 721–732. [PubMed: 32813948]

Yu Q, Yuan L, Deng J, and Yang Q (2015). Lactobacillus protects the integrity of intestinal epithelial barrier damaged by pathogenic bacteria. Front Cell Infect Microbiol 5, 26. [PubMed: 25859435]

Author Manuscript Author Manuscript Author Manuscript Author Manuscript

Zmora N, Suez J, and Elinav E (2019). You are what you eat: diet, health and the gut microbiota. Nat Rev Gastroenterol Hepatol 16, 35–56. [PubMed: 30262901]

Zou J, Chassaing B, Singh V, Pellizzon M, Ricci M, Fythe MD, Kumar MV, and Gewirtz AT (2018). Fiber-Mediated Nourishment of Gut Microbiota Protects against Diet-Induced Obesity by Restoring IL-22-Mediated Colonic Health. Cell Host Microbe 23, 41–53.e44. [PubMed: 29276170]

Author Manuscript Author Manuscript Author Manuscript Author Manuscript

Highlights

- Reg3g is required for metabolic benefits of surgical or dietary interventions
- Surgical or dietary intervention improves gut function in a Reg3g-dependent manner
- Reg3g induction is associated with microbiota altered by surgical or dietary interventions
- Pharmacological application of Reg3g improves glucose tolerance in DIO mice

Author Manuscript Author Manuscript Author Manuscript Author Manuscript

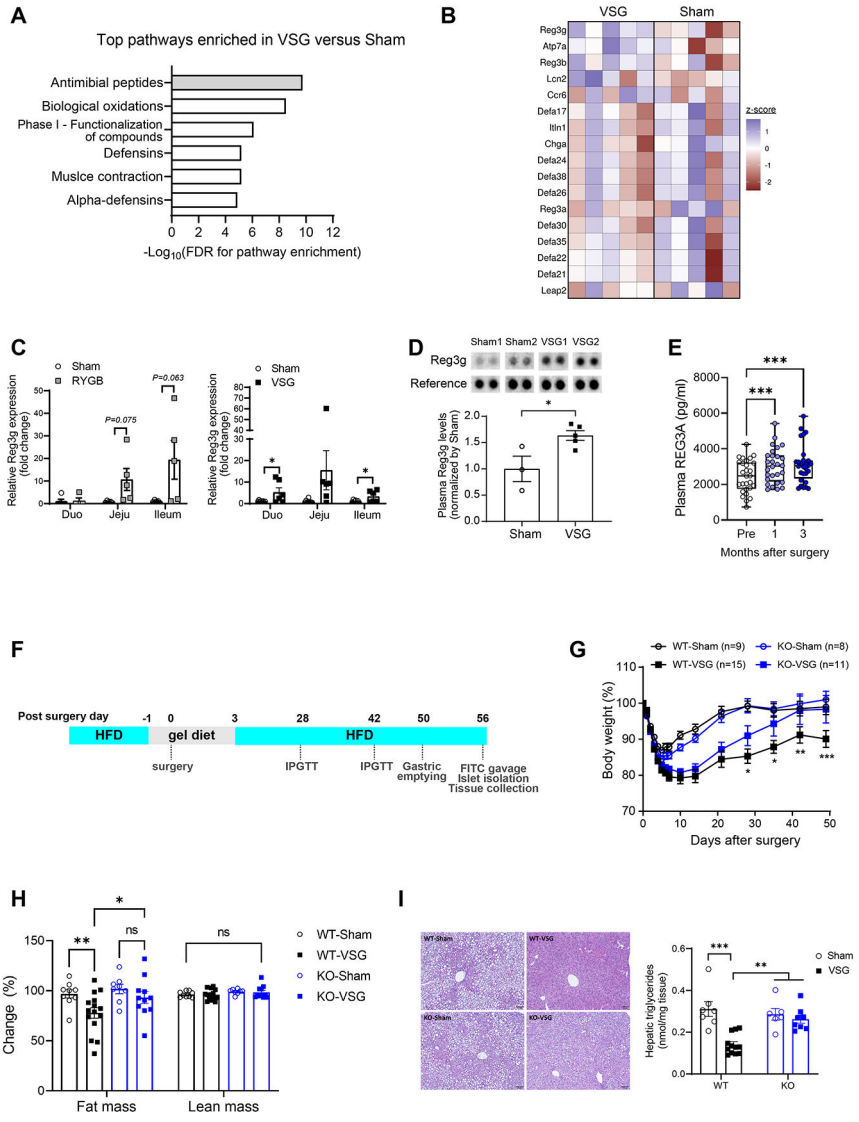

Figure 1. Reg3g is required for the maintenance of weight loss following VSG

(A) Top 6 pathways enriched in the ileum of VSG mice relative to Sham mice. (full dataset available online as NCBI GEO data set-GSE53782) (Ryan et al., 2014).

(B) Gene expression profiles enriched in the antimicrobial peptides pathway (n=5/group). (full dataset available online as NCBI GEO data set-GSE53782).

(C) mRNA expression of Reg3g in the small intestine from rats underwent RYGB (Rat) (n = 5 for both groups) and mice underwent VSG (Sham n = 8; VSG n = 6).

(D) Circulating levels of Reg3g in Sham (n=3) and VSG (n=5)-operated mice.

(E) Circulating REG3A concentrations before and at 1 and 3 months after surgery in young patients who underwent VSG surgery (n=29).

(F) Experimental timeline.

(G) Body weight change (%) of sham and VSG-operated mice over the study period (WT-Sham n=9, WT-VSG n=15, KO-Sham n=8, KO-VSG n=11).

(H) Body composition changes 8 weeks after surgery period (WT-Sham n=9, WT-VSG n=15, KO-Sham n=8, KO-VSG n=11).

Author Manuscript Author Manuscript Author Manuscript Author Manuscript

(I) Representative images of the H&E-stained liver section and quantification of liver triglyceride in mice histopathological examination of liver (n=7 WT-Sham, 12 WT-VSG, 6 KO-Sham, 8 KO-VSG).

Data are shown as means±SEM. *P* values indicate multiple unpaired t test (C), Student's 2-tailed *t* test (D), a repeated-measures 1-way ANOVA (E), or 2-way ANOVA (F, G, and H); *p < 0.05, **p < 0.01, ***p < 0.001.

Author Manuscript Author Manuscript Author Manuscript Author Manuscript

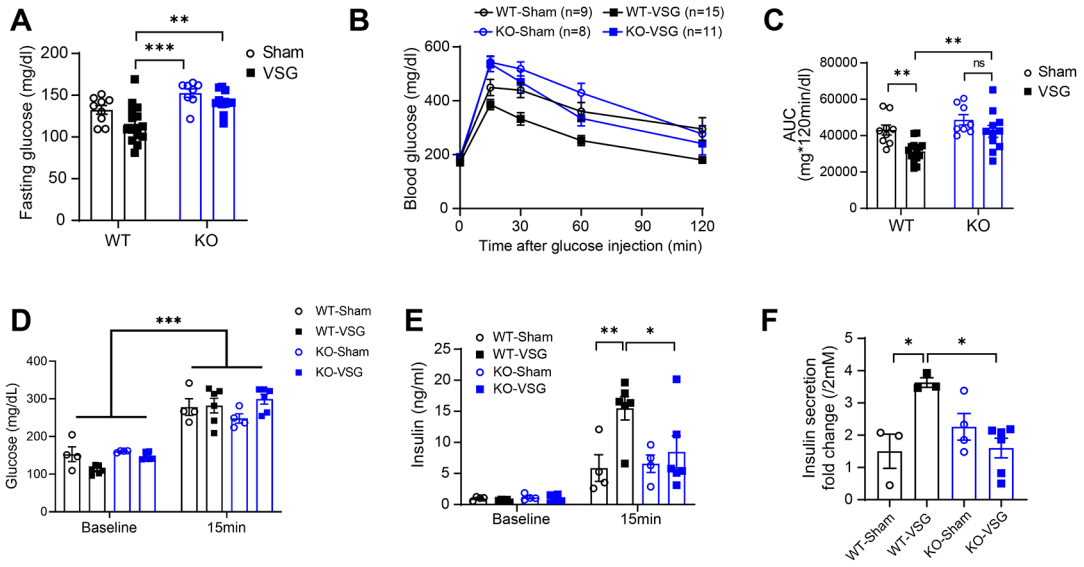

Figure 2. Reg3g enhances glucose homeostasis after VSG

(A) Overnight-fasting glucose levels.

(B) Intraperitoneal tolerance test (IP injection of a bolus of 2g/kg dextrose) was performed at 4 weeks post operation. Blood glucose levels were measured at the indicated point.

(C) Corresponding area under the curve (AUC). (A to C; n=9 WT-Sham, 15 WT-VSG, 8 KO-Sham, 11 KO-VSG).

(D) Blood glucose levels before and 15min post glucose gavage (2g/kg dextrose) from mice underwent intestinal permeability test (Sham n=4; VSG n=6)

(E) Circulating levels of Insulin 15min post glucose gavage (2g/kg dextrose) from mice underwent intestinal permeability test (Sham n=4; VSG n=6).

(F) Glucose (12mM) -stimulated insulin secretion in isolated islets shown as fold change above basal.

Data are shown as means±SEM. *P* values indicate 2-way ANOVA (A, C, D and E) or 1-way ANOVA (F); *p < 0.05, **p < 0.01, ***p < 0.001.

Author Manuscript Author Manuscript Author Manuscript Author Manuscript

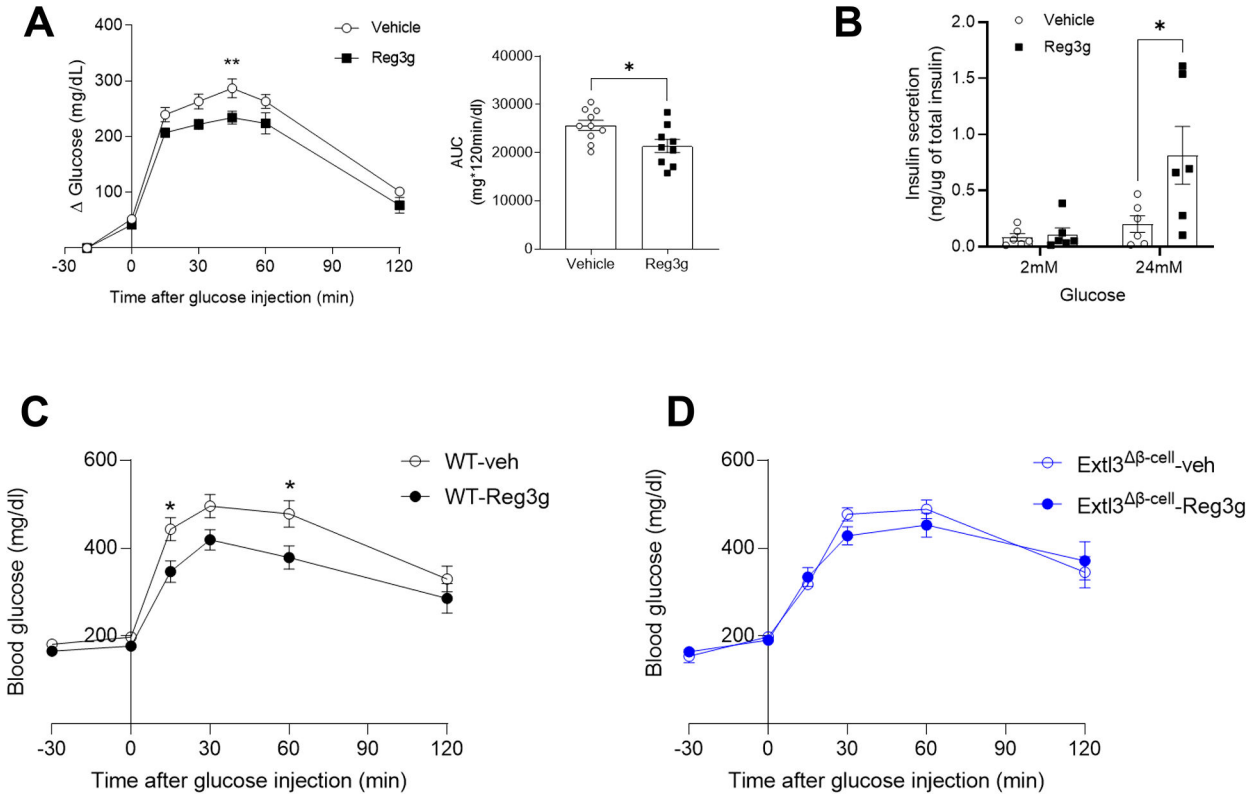

Figure 3. Pharmacological effect of Reg3g on glucose regulation

(A) Effect of acute injection of Reg3g on glucose tolerance. IPGTT in DIO mice 20min after single dose of PBS (n=10) or Reg3g (0.1 mg/kg) (n=9).

(B) Glucose-stimulated insulin secretion in isolated islets from lean WT mice. Islets were incubated for an hour with vehicle or Reg3g (50ng/ml) before glucose treatment.

(C and D) Effect of acute injection of Reg3g on DIO WT (vehicle n=6; Reg3g n=8) (C) and Extl3$^{\Delta\beta\text{-cell}}$ mice (vehicle n=10; Reg3g n=11) (D).

Data are shown as means±SEM. *P* values indicate 2-Way ANOVA or Student's 2-tailed t test; *p < 0.05, **p < 0.01, ***p < 0.001.

Author Manuscript Author Manuscript Author Manuscript Author Manuscript

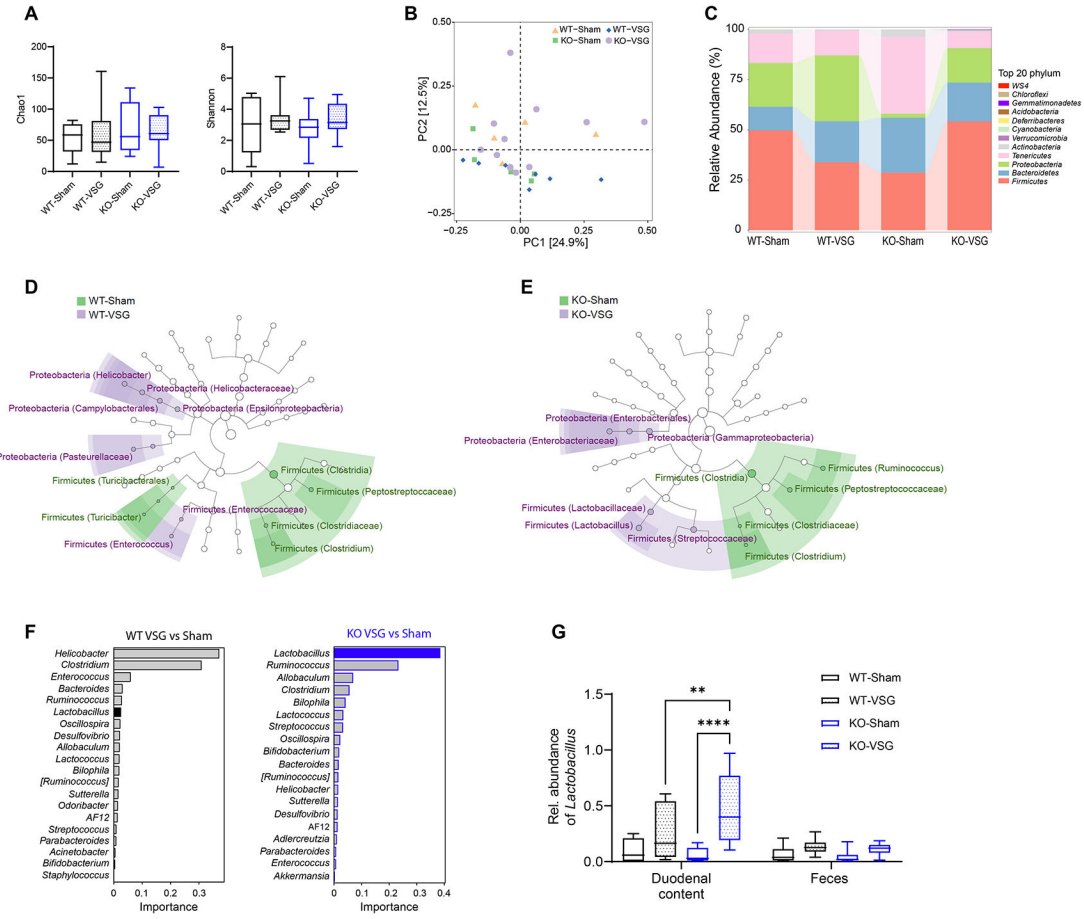

Figure 4. Alteration of Gut microbiota in duodenum of Reg3g KO mice after VSG

(A) Chao1 (richness) and Shannon (diversity) index of the gut microbiota in the duodenal contents.

(B) Principal-coordinate analysis (PCoA) of unweighted UniFrac distances for the duodenal microbiota. Each symbol represents an individual mouse.

(C) Average relative abundance of bacterial phyla in duodenal contents from VSG or Sham operated mice.

(D and E) LEfSe analysis depicting nodes within the bacterial taxonomic hierarchy that are enriched in duodenal microbiota from WT-VSG versus WT-Sham (D) and KO-VSG versus KO-Sham (E). Cladogram generated by LEfSe indicating differences at phylum, class, order, family, and genus levels between the two groups.

(F) Discriminatory importance scores of top-ranked genus identified by the Random Forest analysis. A comparison of the abundance of markers in WT-VSG (left) and KO-VSG (right) relative to Sham counterparts.

(G) Relative abundance of *Lactobacillus* genus in the duodenal contents and feces.

Data are shown as means±SEM; WT-Sham n=5, WT-VSG n=7, KO-Sham n=5, KO-VSG n=12. *P* values indicate 2-way ANOVA; *p < 0.05, **p < 0.01, ***p < 0.001.

Author Manuscript
Author Manuscript
Author Manuscript
Author Manuscript

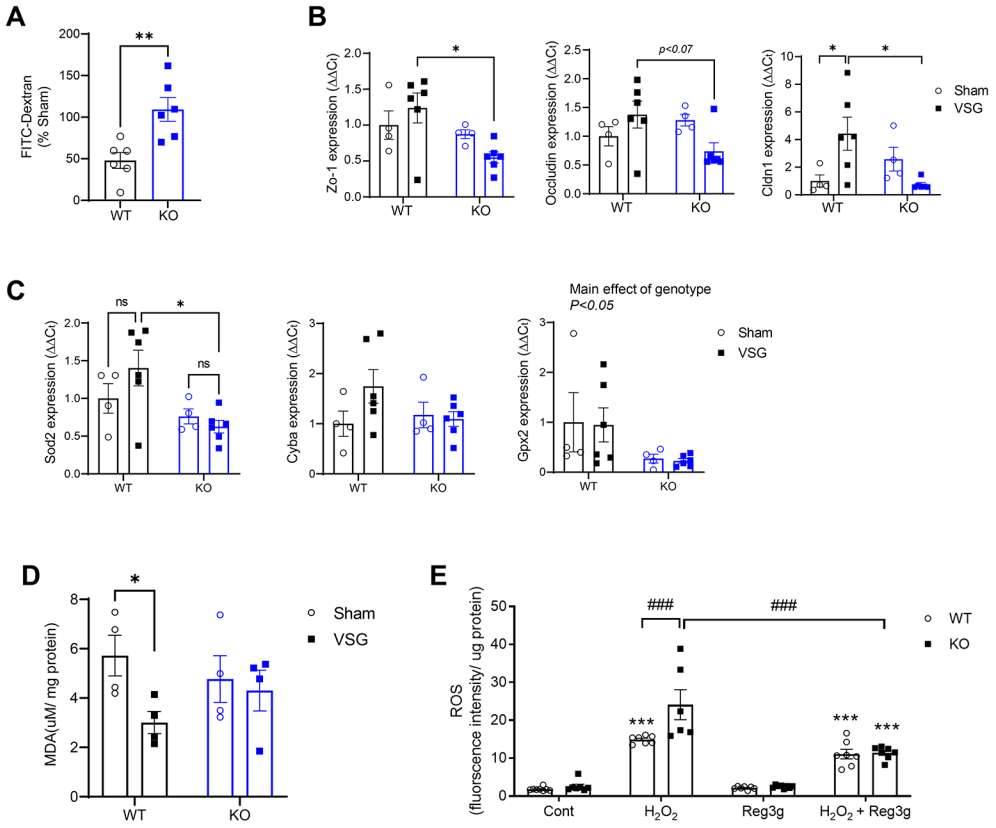

Figure 5. Reg3g contributes to improvements in gut function after VSG

(A) Intestinal permeability determined by FITC-dextran in VSG-operated mice as % change (Sham-operated mice) (n=6).

(B) Expression of genes involved in intestinal cell integrity in intestine from Sham and VSG-operated mice underwent intestinal permeability test (Sham n=4/genotype, VSG n=6/genotype).

(C) Expression of genes involved in anti-oxidative stress from Sham and VSG-operated mice underwent intestinal permeability test (Sham n=4/genotype, VSG n=6/genotype).

(D) MDA concentrations in the ileum from HFD fed WT and Reg3g KO mice after surgery (n=4/group).

(E) Measurement of Cellular ROS production in the enteroids at 2h with H_2O_2 (200μM) in ± Reg3g (100 ng/ml) (n=7/treatment). ***p < 0.001 for control versus H_2O_2; ###p < 0.001. Data are shown as means±SEM. *P* values indicate Student's 2-tailed t test(A) or 2-way ANOVA (B, C, D, and E); *p < 0.05, **p < 0.01, ***p < 0.001.

Author Manuscript Author Manuscript Author Manuscript Author Manuscript

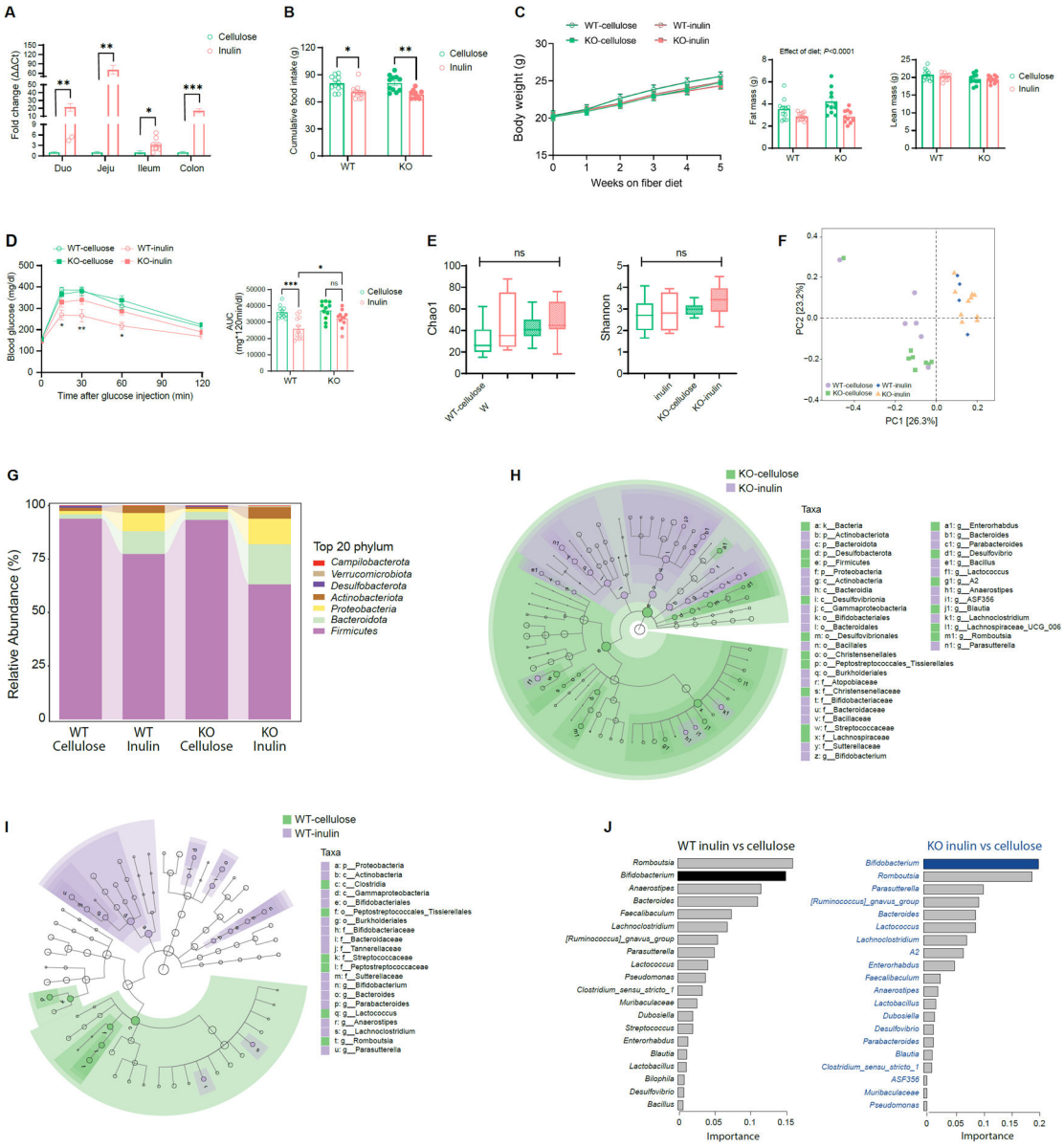

Figure 6. Contribution of Reg3g to metabolic improvements induced by fermentable Inulin supplement

(A) mRNA expression of Reg3g in the intestinal segments from mice fed a cellulose or inulin diet (cellulose n=7, inulin n=8).

(B) Cumulative food intake of WT and Reg3g KO mice on a cellulose or inulin-enriched diet (WT n=12/diet, KO n=11/diet).

(C) Body weight and body composition over time.

(D) IPGTT (IP injection of a bolus of 2g/kg dextrose) was performed. Blood glucose levels were measured at the indicated point and area under curve (AUC).

(E) Chao1 richness and Shannon diversity of the gut microbiota in the duodenal contents.

(F) Principal-coordinate analysis (PCoA) of unweighted UniFrac distances for the duodenal microbiota. Each symbol represents an individual mouse.

Author Manuscript Author Manuscript Author Manuscript Author Manuscript

(G) Average relative abundance of bacterial phyla in duodenal contents from cellulose- or inulin-diet fed mice (WT-cellulose n=6, WT-inulin n=4, KO-cellulose n=8, KO-inulin n=10).
(H and I) LEfSe analysis depicting nodes within the bacterial taxonomic hierarchy that are enriched in duodenal microbiota from KO cellulose versus inulin (H) and WT cellulose versus inulin (I). Cladogram generated by LEfSe indicating differences at phylum, class, order, family, and genus levels between the two groups.
(J) Discriminatory importance scores of top-ranked genus identified by the Random Forest analysis. A comparison of the abundance of markers in WT-inulin (left) and KO-inulin (right) relative to cellulose-fed counterparts.
Data are shown as means±SEM. *P* values indicate 2-way ANOVA (A and E) or multiple unpaired t test (B); *p < 0.05, **p < 0.01, ***p < 0.001.

Author Manuscript Author Manuscript Author Manuscript Author Manuscript

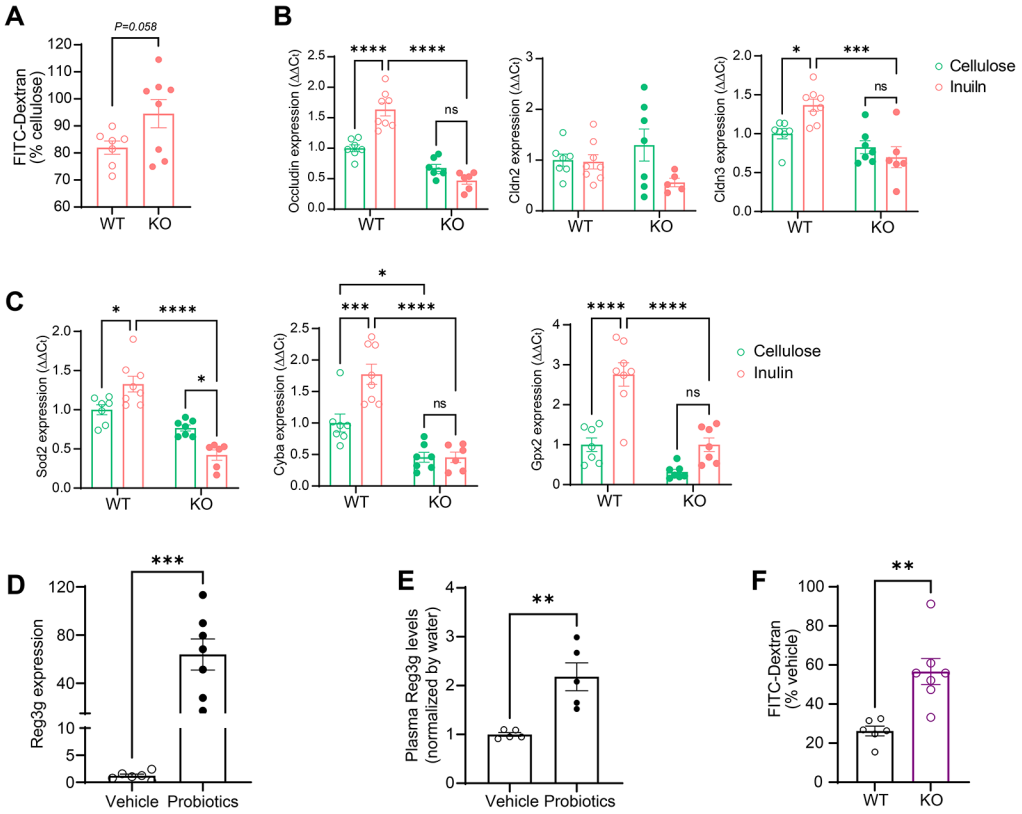

Figure 7. Reg3g contributes to improvements in gut function mediated by microbiota

(A) Intestinal permeability determined by FITC-dextran in inulin-fed mice as % change (cellulose-fed mice) (n=7-8).

(B) Expression of genes involved in intestinal cell integrity in intestine from cellulose or inulin-fed mice (n=6-8).

(C) Expression of genes involved in anti-oxidative stress in intestine from cellulose or inulin-fed mice (n=6-8).

(D) Expression of intestinal Reg3g in mice given PBS or probiotics (n=6-7)

(E) Circulating levels of Reg3g in mice given PBS or probiotics (n=5).

(F) Intestinal permeability determined by FITC-dextran in probiotics-gavage mice given LPS (0.1 mg/kg) as % change (vehicle-fed mice) (n=6-7).

Data are shown as means±SEM. *P* values indicate Student's 2-tailed t test (A, D, and E) or 2-way ANOVA (B and C); *p < 0.05, **p < 0.01, ***p < 0.001.

Author Manuscript Author Manuscript Author Manuscript Author Manuscript

KEY RESOURCES TABLE

REAGENT or RESOURCE	SOURCE	IDENTIFIER
Bacterial and Virus Strains		
VSL#3	Sigma-TauPharmaceuticals	N/A
Chemicals, Peptides, and Recombinant Proteins		
RPMI 1640 Medium	Thermo Fisher Scientific	Cat# 11875093
FBS	Thermo Fisher Scientific	Cat# 10-082-147
HBSS	Thermo Fisher Scientific	Cat# 14025092
Penicillin-Streptomycin	Thermo Fisher Scientific	Cat# 15140122
Collagenase P,from Clostridium	Roche	Cat# 11213865001
Fluorescein isothiocyanate-dextran	Sigma-Aldrich	Cat# FD4
Lipopolysaccharides from Escherichia coli O111:B4	Sigma-Aldrich	Cat# L2630-10MG
Acetaminophen	Sigma-Aldrich	Cat# A7085
Cellytic™ M,Cell Lysis Reagent	Sigma-Aldrich	Cat# C2978-250ML
cOmplete™ Protease Inhibitor Cocktail	Sigma-Aldrich	Cat# 11697498001
Power SYBR™ Green PCR Master Mix	Applied Biosystems	Cat# 4367659
iScript cDNA synthesis kit	BioRad	Cat# 170-8891
SsoAdvanced Universal Probe Supermix	BioRad	Cat# 1725284
Critical Commercial Assays		
Ultra Sensitive Mouse Insulin ELISA	Crystal Chem	Cat# 90080; RRID:AB_2783626
Total GLP-1 kit	Mesoscale Discovery	Cat# K150JVC-1; RRID: AB_2801383
Human Reg3α antibody set	Mesoscale Discovery	Cat# F21U8-3
Proteome Profiler Mouse XL Cytokine Array	R&D Systems	Cat# ARY028
Pure Link RNA mini kit	Thermo Fisher Scientific	Cat# 12183025
Acetaminophen-L3K	Sekisui Diagnostics	Cat# 506-30
Lipid extraction kit	Abcam	Cat# ab211044
Triglyceride Quantification Colorimetric/Fluorometric kit	Biovision	Cat# K622
Oxiselect TBARS assay kit	Cell Biolabs	Cat# STA-330
DCFDA/H2DCFDA assay kit	Abcam	Cat# ab113851
MagAttract PowerMicrobiome kit DNA/RNA kit	Qiagen	Cat# 27500-4-EP
MiSeq V2 Reagent kit	Illumina	Cat# MS-102-2003
Bioanalyzer High Sensitivity DNA Analysis	Agilent	Cat# 5067-4626
Deposited Data		
RNA-seq of ileum following VSG and pair-fed sham surgery	(Ryan et al., 2014)	GSE53782
Experimental Models: Organisms/Strains		
Mouse: Reg3g KO mice	Lora V. Hooper Lab	N/A
Mouse: Extl3 flox/flox mice	Akira Sugawara Lab	N/A
Mouse: Ob/Ob: Cg-Lepob/J	The Jackson Laboratory	Stock No: 000632; RRID:IMSR_JAX:0 00632
Mouse: C57BL/6J	The Jackson Laboratory	Stock No: 000664; RRID:IMSR_JAX:0 00664

Author Manuscript Author Manuscript Author Manuscript Author Manuscript

REAGENT or RESOURCE	SOURCE	IDENTIFIER
Mouse: B6.Cg-Tg(Ins1-cre/ERT)1Lphi/J	The Jackson Laboratory	Stock No: 026802; RRID:IMSR_JAX: 026802
Oligonucleotides		
See Table S1		
Software and Algorithms		
ImageJ	NIH	https://imagej.nih.gov/ij/
GraphPad Prism 8	GraphPad Software	https://www.graphpad.com
R3.6.3	The R Foundation	https://www.r-project.org/
ReactomePA	(Yu and He, 2016)	https://www.bioconductor.org/packages/release/bioc/html/ReactomePA.html
STAR 2.7.3a	(Dobin et al., 2012)	https://github.com/alexdobin/STAR/releases
Other		
Cell Strainers 70μm	Thermo Fisher Scientific	Cat# 07-201-431
Millicell Cell Culture Insert	Millipore	Cat# PI8P01250
Regular chow diet	Envigo Teklad	Cat# 7012
High Fat Diet	Research Diets	Cat# D12492
Cellulose-enriched high-fat diet	Research Diets	Cat. # D13081107
Inulin-enriched high-fat diet	Research Diets	Cat. # D13081106
Pure carbohydrate	Harlan Teklad	Cat# TD02521
Pure fat	Harlan Teklad	Cat# TD02522
Pure protein	Harlan Teklad	Cat# TD02523
DietGel® Boost (for postoperative care)	ClearH_2O	Cat# 72-04-5022
Ensure® Plus (for liquid mixed-nutrient gavage)	Abbott Laboratories	N/A
Biosen C-Line Glucose analyzer	EKF Diagnostics	N/A